

Cover Page



Universiteit Leiden



The handle <http://hdl.handle.net/1887/29080> holds various files of this Leiden University dissertation

**Author:** Fan, Yuanwei

**Title:** The role of AGC3 kinases and calmodulins in plant growth responses to abiotic signals

**Issue Date:** 2014-10-15

## Chapter 2

# **TOUCHing PINOID: a calmodulin–kinase interaction modulates auxin transport polarity during root gravitropism**

Yuanwei Fan<sup>1</sup>, Carlos Samuel Galván-Ampudia<sup>1,2,3</sup>, Hédère S. Robert<sup>1,2,4</sup>, Karen Sap<sup>1</sup>, Elco Backus<sup>1</sup>, Remko Offringa<sup>1,5</sup>

<sup>1</sup> Molecular and Developmental Genetics, Institute Biology Leiden, Leiden University, Sylviusweg 72, 2333 BE Leiden, The Netherlands

<sup>2</sup> These authors contributed equally to this manuscript

<sup>3</sup> Present address: Laboratoire de Reproduction et Développement des Plantes, CNRS, INRA, ENS Lyon, UCBL, Université de Lyon, 69364 Lyon, France

<sup>4</sup> Present address: Mendel Centre for Genomics and Proteomics of Plants Systems, CEITEC MU - Central European Institute of Technology, Masaryk University, CZ-625 00 Brno, Czech Republic.

<sup>5</sup> Author for correspondence ([r.offringa@biology.leidenuniv.nl](mailto:r.offringa@biology.leidenuniv.nl))



## Summary

The plant hormone auxin is well-known to cause elevated cytosolic  $\text{Ca}^{2+}$  levels ( $[\text{Ca}^{2+}]_{\text{cyt}}$ ), however, how  $\text{Ca}^{2+}$  signaling assists in auxin-mediated plant development and growth is not well understood. Here we show that the Arabidopsis plasma membrane (PM)-associated kinase PINOID (PID), a key-determinant in the polar subcellular targeting of PIN auxin efflux carriers, interacts in an auxin-induced,  $\text{Ca}^{2+}$ -dependent manner with the calmodulin-like protein CML12/TCH3. This interaction results in dissociation of the PID kinase from the PM to the cytosol, away from its PIN phosphorylation targets. During root gravitropism, elevated  $[\text{Ca}^{2+}]_{\text{cyt}}$  and TCH3 levels act downstream of auxin to trigger PID internalization followed by PIN2 depolarization, which enhances root gravitropism by maximizing the differential auxin response in the root tip. The dynamic  $\text{Ca}^{2+}$ /CML-dependent shuttling of PID between PM and cytosol reveals a novel regulatory mechanism through which auxin modulates the direction of its own transport.

## Introduction

$\text{Ca}^{2+}$  plays an important role as intracellular second messenger in a variety of signaling pathways. In plants, rapid changes in the cytosolic  $\text{Ca}^{2+}$  concentration ( $[\text{Ca}^{2+}]_{\text{cyt}}$ ) are required for the transduction of both abiotic signals and biotic stimuli (Bouché et al., 2005). In order to give an appropriate response, cells need to distinguish the  $\text{Ca}^{2+}$  signals produced by these different stimuli. Spatial and temporal patterns of  $\text{Ca}^{2+}$  responses, and also the presence of  $\text{Ca}^{2+}$  “receptors” or sensors in the cell, are needed to give specificity to the signal (Luan et al., 2002; Sanders et al., 2002). A major group of  $\text{Ca}^{2+}$  receptor proteins monitor changes in the  $[\text{Ca}^{2+}]_{\text{cyt}}$  through helix-loop-helix  $\text{Ca}^{2+}$  binding domains called EF-hands (Strynadka and James, 1989). The conformational changes induced by binding of  $\text{Ca}^{2+}$  to these proteins either induce their activation, or enhance their interaction with other proteins that are in turn activated or repressed (Travé et al., 1995; Luan et al., 2002; Sanders et al., 2002). Two main types of EF hand proteins are known: the calmodulins (CaMs) and the  $\text{Ca}^{2+}$ -dependent protein kinases (CDPKs). CaMs are small proteins with typically four EF-hands without an effector domain that are highly conserved in all eukaryotes. Plant genomes, however, also encode a large number of CaM-like proteins (CMLs) that in most cases also have 4 EF-hands, and seem to act in a similar manner as CaMs (McCormack and Braam, 2003; Hashimoto and Kudla, 2011). The transmission of the  $\text{Ca}^{2+}$  signal occurs through the interaction with target proteins to influence their activity (Snedden and Fromm, 2001; Bouché et al., 2005). The CDPKs combine a calmodulin-like domain with a kinase domain. Binding of  $\text{Ca}^{2+}$  directly activates the protein kinase (Cheng et al., 2002).

The phytohormone auxin regulates plant development by controlling basic cellular processes such as cell division, -differentiation and -elongation (Reinhardt et al., 2000; Nakajima and Benfey, 2002; Weijers and Jurgens, 2005; Peret et al., 2009). Ever since the first observations of Darwin on the growth response of Canary grass coleoptiles to unidirectional light (Darwin, 1880), it is well-established that auxin is transported from cell to cell in a polar fashion from its sites of synthesis to its sites of action (Tanaka et al., 2006; Petrasek and Friml, 2009; Vanneste and Friml, 2009; Ljung, 2013). This polar auxin transport (PAT) generates auxin gradients and maxima that mediate photo- and gravitropic growth responses, and are instructive for embryogenesis, meristem maintenance and organ positioning (Sabatini et al., 1999; Friml et al., 2002; Benkova et al., 2003; Friml et al., 2003; Reinhardt et al., 2003). The mechanism of auxin transport has been intensely studied, and PIN transmembrane proteins have been identified as auxin efflux carriers that direct this polar cell-to-cell transport through their asymmetric

subcellular localization (Petrasek et al., 2006; Wisniewska et al., 2006). The plant-specific AGC serine/threonine protein kinase PINOID (PID) was identified as a regulator of auxin transport (Benjamins et al., 2001) Together with two close homologs WAG1 and WAG2, PID directs PIN polar localization at the apical (shootward) cell membrane, by phosphorylation of the serines in three conserved TPRXS motifs of the PIN central hydrophilic loop (Friml et al., 2004; Michniewicz et al., 2007; Dhonukshe et al., 2010; Huang et al., 2010).

Several studies suggest that the auxin signaling pathway involves rapid changes in the  $[Ca^{2+}]_{cyt}$ . For example, in wheat protoplasts (Shishova and Lindberg, 2004), maize coleoptile cells (Felle, 1988; Gehring et al., 1990a) and parsley cells (Gehring et al., 1990a), an increase of the  $[Ca^{2+}]_{cyt}$  was detected within minutes after auxin application using  $Ca^{2+}$  fluorescent dyes or ion-sensitive microelectrodes. Also, an auxin-induced  $Ca^{2+}$  pulse was observed in intact plant tissues such as maize and pea roots (Gehring et al., 1990a) and  $Ca^{2+}$  has been implied as an important signal in the regulation of PAT in sunflower hypocotyls (dela Fuente and Leopold, 1973), in gravistimulated roots (Lee and Evans, 1985; Monshausen et al., 2008; Monshausen et al., 2011) and during phototropism (Baum et al., 1999; Harada and Shimazaki, 2007). In gravitropic root growth, the gravity vector is perceived by the interaction between statoliths and the cytoskeleton in the columella root cap cells, leading to a local  $Ca^{2+}$  response. Initial experiments by Lee et al. (Lee et al., 1984; Lee and Evans, 1985) suggested that  $Ca^{2+}$  transport across the root tip plays an important role and that  $Ca^{2+}$  in the elongation zone enhances auxin transport in horizontally placed root tips. Although the exact order of events is still unknown, the use of the Yellow Cameleon  $Ca^{2+}$  reporter YC3.6 has shown that gravitropic growth and auxin induce elevated  $[Ca^{2+}]_{cyt}$  in epidermis cells at the lower side of the root (Monshausen et al., 2011). For phototropic growth, the blue light signal perceived by the phototropin receptor kinases phot1 and phot2 induces a rapid increase in  $[Ca^{2+}]_{cyt}$  (Baum et al., 1999; Harada et al., 2003; Zhao et al., 2013) and triggers PIN-dependent auxin accumulation at the shaded side, leading to shoot bending toward the light source (Friml et al., 2002; Esmon et al., 2006; Ding et al., 2011). Although the  $Ca^{2+}$  response does not seem to be required for phot1-mediated phototropic response to low fluence rate blue light (Folta et al., 2003), it seems to be essential for the phot1- and phot2-mediated phototropic response to higher fluence rate blue light (Zhao et al., 2013). The PHYTOCHROME KINASE SUBSTRATE 1 protein (PKS1) was found to interact with phot1 (Lariguet et al., 2006) and to act redundantly with PKS2 and PKS4, which is downstream of  $Ca^{2+}$  signaling, possibly through its

interaction with CAM4 (Zhao et al., 2013).

Our previous finding found that PID interacts in a  $\text{Ca}^{2+}$ -dependent manner with the EF-hand protein PINOID BINDING PROTEIN1 (PBP1) and the CML TOUCH3 (TCH3/CML12) provided the first molecular evidence for  $\text{Ca}^{2+}$  as a signal transducer in the regulation of PAT (Benjamins et al., 2003). In *Arabidopsis*, TCH3 is unique in that it has 6 instead of the 4 EF-hand motifs generally predicted in CaMs and CMLs. Its corresponding gene was initially identified as a touch-responsive gene (Braam and Davis, 1990; Sistrunk et al., 1994). Here we present a detailed study of the *in vivo* interaction between PID and TCH3. Using loss- and gain-of-function mutant lines, we confirm *in vitro* observations that TCH3 is a negative regulator of the PINOID kinase activity. This regulation occurs directly by inhibition of the kinase activity, as shown in phosphorylation assays, and by sequestration of PID from the plasma membrane (PM) where its phospho-targets the PIN proteins are located (Michniewicz et al., 2007; Huang et al., 2010). We also show that the PID-TCH3 signaling complex plays a role in fine-tuning root growth, e.g. during root gravitropism where PID internalization triggered by the auxin-induced  $\text{Ca}^{2+}$  response at the lower side of the root leads to PIN2 apolarity, which is needed for maximization of the differential auxin distribution, and thus the gravitropic response.

## Results

### TCH3 reduces kinase activity by binding to the PID catalytic domain

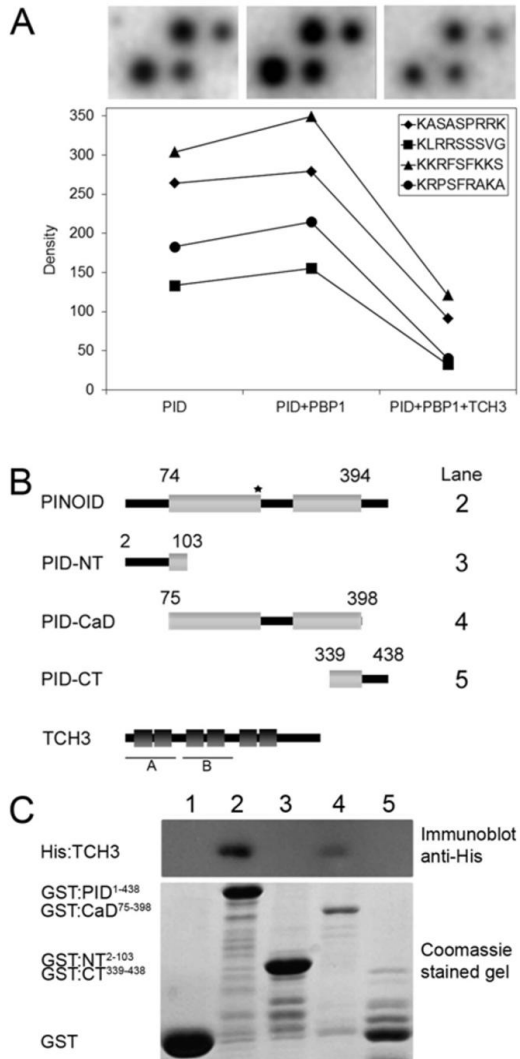


**Figure 1 TCH3 reduces PID activity by interacting with its catalytic kinase domain.**

(A) Detail of a phospho-peptide chip incubated with radiolabelled ATP and either PID alone, PID and the positive regulator PBP1, or PID, PBP1 and TCH3. Densitometry analysis of the four spots in the upper images is provided in the graph below. The density value indicates the number of black grains in the measured circle.

(B, C) Mapping the TCH3 interaction domain in PID with *in vitro* pull downs (B) Schematic representation of PID (498 aa), or its N-terminal portion (PID-NT, aa 2-103), the catalytic domain (PID-CaD, aa 75-398), or the C-terminal portion (PID-CT, aa 339-438), and TCH3 (324 aa). The light grey boxes in PID represent the kinase catalytic core (aa 74-394), which in PID has an amino acid insertion between sub-domain VII and VIII (aa 226-281). The star indicates the position of the DFG to DFD mutation characteristic for the plant-specific AGCVIII protein kinases. The six EF-hand domains in TCH3 (aa 11-38, 50-74, 101-127, 139-163, 191-217, 228-253) are depicted as dark grey boxes. A and B indicate an exact duplication of two EF-hand domains in TCH3.

(C) Western blot analysis (top panel) following pull-down with GST-tagged PID or deletion versions thereof. Lane 1 is the pull down with GST alone. Other lane numbers refer to the GST-PID versions depicted in (B). Coomassie stained gel (bottom panel) showing the input of proteins used in the pull-down assay.

Previous *in vitro* pull-down assays showed that the PID kinase-TCH3 CML interaction is  $\text{Ca}^{2+}$ -dependent (Benjamins et al., 2003). Moreover, a traditional kinase assay with Myelin Basic Protein (MBP) as substrate showed that TCH3 reduces the *in vitro* phosphorylation activity of PID (Benjamins et al., 2003). To confirm the effect of TCH3 on PID activity with a wider array of substrates, we incubated a commercial phospho-peptide chip with radiolabelled ATP and PID. For a quantitative comparison of differences in PID activity, we focused on the phosphorylation intensity of four peptides, including a phospho-target in MBP. PID efficiently phosphorylated all four peptides (Figure 1A). In the presence of the single EF-hand protein PBP1, a positive regulator of PID activity (Benjamins et al., 2003), the phosphorylation intensity was significantly increased (Figure 1A). Addition of TCH3 to the PID and PBP1 containing mix reduced the phosphorylation intensity significantly reduced to even below the basal phosphorylation level by PID alone (Figure 1A). These data corroborate the conclusions of our previous analysis that TCH3 is a negative regulator of PID kinase activity *in vitro*, and indicate that TCH3 binding to PID is able to overrule the positive effect of PBP1.

In order to roughly map the TCH3 interaction site in PID, *in vitro* pull-down assays were performed using GST-tagged isolates of the N-terminal domain (aa 2-103), the catalytic domain (aa 75-398) or the C-terminal domain (aa 339-438) of PID, along with its full-length version to test their interaction with crude *E. coli* extracts containing histidine (His)-tagged TCH3 (Figure 1B, C). Immuno-detection of His-TCH3 after GST pull-down indicated that TCH3 interacts with full-length PID or its catalytic domain (Figure 1C, lanes 2 and 4) but not with the N- or C-terminal domains (Figure 1C, lanes 3 and 5). Binding of TCH3 to the PID catalytic domain provided an explanation why this interaction affected PID kinase activity in the phosphorylation assays (Figure 1A).

## TCH3 mediates auxin-dependent sequestration of PID from the PM

Transfection of *Arabidopsis* protoplasts with a *35S::TCH3-YFP* construct showed that the fusion protein, like soluble CFP, is cytoplasmic, but unlike CFP it is excluded from the nucleus (Figure 2A, upper panel). A similar localization was observed for the TCH3-mRFP fusion protein in root epidermis cells of *TCH3::TCH3-mRFP* seedlings (Figure 2B, right panel). In contrast, PID showed predominant membrane-association and partial cytosolic localization both in protoplasts (Figure 2B, left panel) and *in planta* (Figure 2B, middle panel), in accordance with previously published data (Lee and Cho, 2006; Michniewicz et al., 2007).

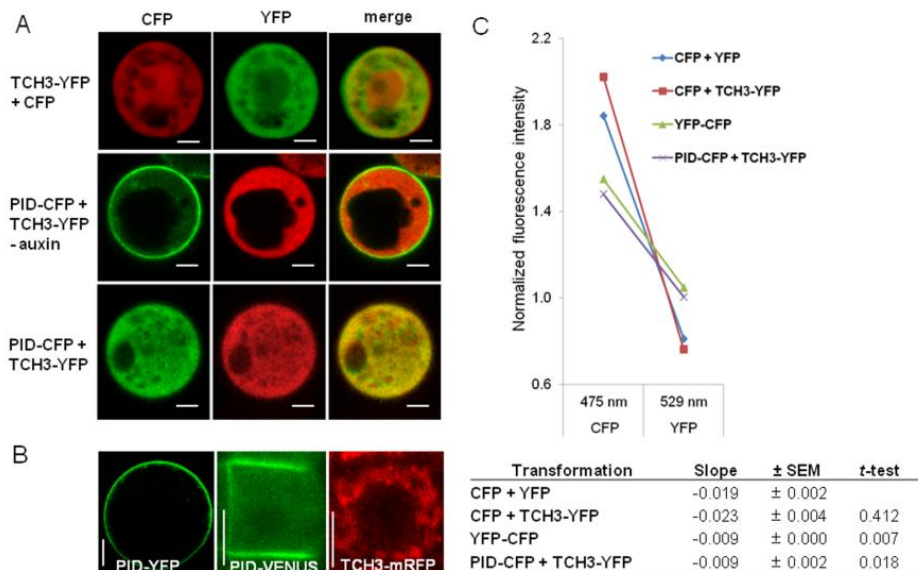


**Figure 2 Auxin-dependent interaction with TCH3 sequesters PID from the PM to the cytosol in *Arabidopsis* protoplasts.**

(A) The indicated YFP and CFP fusion proteins were (co-)expressed from *35S* promoter-driven constructs, and CFP channel-, YFP channel-, and merged images of representative protoplasts are shown per transfection. TCH3-YFP is cytoplasmic and unlike CFP excluded from the nucleus (1st row). In auxin-starved protoplasts, PID-CFP localizes to the plasma membrane (PM) and TCH3-YFP to the cytosol (2nd row), however, when protoplasts are cultured in the presence of NAA, PID co-localizes with TCH3 in the cytosol (3rd row).

(B) PID-YFP expressed in auxin-cultured cells shows clear PM localization (left image). In root epidermis cells PID-VENUS also shows predominant PM localization (middle image), whereas TCH3-mRFP is

localized in the cytosol (right image).

(C) Fluorescence resonance energy transfer (FRET) analysis by lambda scanning of 3 separate locations in 3 different representative protoplasts. The graph shows the average normalized fluorescence intensities (see materials and methods) at 475 nm (CFP emission peak) and 529 nm (YFP emission peak) using an excitation wavelength of 457 nm (donor, CFP) in *Arabidopsis* protoplasts co-expressing CFP and YFP (diamond, blue line, negative control), CFP and TCH3-YFP (square, red line, negative control), a translational fusion between YFP and CFP (triangle, green line, positive control), or PID-CFP and TCH3-YFP (cross, purple line). The significant decrease in the slopes of the lines representing the PID-CFP and TCH3-YFP co-expressing and the YFP-CFP expressing protoplasts compared to those of the negative controls (Table, Student's *t*-test,  $p < 0.05$ ) is indicative for the occurrence of FRET. Size bars in A and B are 10  $\mu\text{m}$ .

When the *35S::PID-CFP* and *35S::TCH3-YFP* constructs were cotransfected in auxin-starved *Arabidopsis* protoplasts, PID-CFP and TCH3-YFP remained at their respective subcellular location, showing only weak overlap in the cytosol (Figures 2A, middle panel). However, when cells were cultured in normal auxin-containing medium, PID-CFP showed predominant cytosolic localization in the presence of TCH3-YFP (Figures 2A, lower panel), suggesting that an auxin-dependent interaction with TCH3 sequestered PID from the PM.

To confirm the *in vivo* interaction between the two proteins, we checked for Förster (Fluorescence) Resonance Energy Transfer (FRET) between the CFP and YFP moieties of the co-expressed fusion proteins using confocal lambda scanning (Siegel et al., 2000). No acceptor spectral bleed-through occurred in control protoplasts co-expressing cytosolic CFP and YFP, meaning that YFP (excitation of 514 nm) was not excited by the CFP excitation wavelength (457 nm) and vice versa (data not shown). However, excitation with 457 nm led to a significant CFP-derived signal at the YFP emission wavelength (529 nm) in the samples where *35S::PID-CFP* and *35S::TCH3-YFP* were co-transfected (Figure 2C). The significant FRET signal in these samples was characterized by a quenched signal at the CFP emission wavelength (475 nm) and an enhanced signal at the YFP emission wavelength (527 nm), as compared to control transfections with non-interacting versions of CFP and YFP (*35S::CFP* co-transfected either with *35S::TCH3-YFP* or with *35S::YFP*). The lambda scanning profile matched that of protoplasts expressing a YFP-CFP fusion protein for which FRET is expected (Figures 2C). These data corroborate our earlier hypothesis that TCH3 sequesters PID from the PM to the cytoplasm upon interacting with the protein kinase.

### The PID homolog WAG2 also interacts with TCH3

In view of the functional redundancy between PID and its close homologs (Dhonukshe et al., 2010), we analyzed whether the AGC3 kinases WAG1, WAG2 and AGC3-4 interact with TCH3 by *in vitro* pull-down assays. A His-tagged version of TCH3 was pulled down with GST-PID and -WAG2, but not with GST-WAG1 or GST alone. A very weak band could be observed in the pull down with AGC3-4, suggesting a weak interaction between this kinase and TCH3 (Supplementary Figure S1A).

To confirm these findings *in vivo*, we performed FRET and sequestration analysis on auxin-cultured *Arabidopsis* protoplasts co-expressing the kinase-CFP and TCH3-YFP fusion proteins. A significant relative FRET signal could be detected in protoplasts that co-expressed TCH3-YFP and PID-CFP or WAG2-CFP, whereas co-expression of TCH3-YFP with WAG1-CFP or AGC3-4-CFP resulted in background FRET levels (Supplementary Figure S1B). As observed before (Figure 2A), PID-CFP was sequestered by TCH3-YFP from the PM to the cytoplasm, and the same was observed for WAG2-CFP (Supplementary Figure S1C). In contrast, WAG1-CFP remained at the PM, corroborating the previous *in vitro* pull down and FRET results that WAG1 does not interact with TCH3. Also for AGC3-4-CFP no clear change in subcellular localization could be observed (Supplementary Figure S1C). This latter kinase, however, already showed strong cytosolic and nuclear localization (Supplementary Figure S1C), so it is difficult to draw any conclusion for this kinase from this specific experiment. These data indicate that TCH3 interacts significantly with PID and WAG2 to regulate the activity of these AGC3 kinases in response to changes in  $[Ca^{2+}]_{\text{cyt}}$ .

### Auxin-induced sequestration of PID in root epidermis cells is $Ca^{2+}$ - and TCH3-dependent

Previous studies already indicated that expression patterns of *PID* and *TCH3* overlap (Sistrunk et al., 1994; Antosiewicz et al., 1997; Benjamins et al., 2001; Michniewicz et al., 2007). As shown by a *TCH3::TCH3-GUS* translational fusion, *TCH3* is expressed in epidermis cells of the root elongation zone (Supplementary Figure S2A). Upon IAA or NAA treatment for 1 hour, *TCH3* expression was strongly induced in the root tip, and extended to the vasculature and the epidermis of the complete root (Supplementary Figures S2B, G). Also the *PID* gene is auxin responsive and expressed in epidermis cells in the elongation zone of the root tip ((Benjamins et al., 2001; Michniewicz et al., 2007); Figure 3A, 7A) implying the possibility of a functional *in vivo* interaction

between the two proteins in these cells. Interestingly, in the same cells auxin treatment triggers a rise in  $[Ca^{2+}]_{cyt}$  within seconds and pre-treatment with the  $Ca^{2+}$  channel blocker lanthanum chloride ( $LaCl_3$ ) completely inhibits these auxin-induced  $Ca^{2+}$  transients (Monshausen et al., 2011). Based on these data we hypothesized that the auxin-induced, TCH3-dependent sequestration of PID observed in protoplasts should also occur in root epidermis cells. To test our hypothesis we used the *PID::PID-VENUS* line (Michniewicz et al., 2007). Without any treatment PID-VENUS localized both at the PM and in the cytoplasm (Figure 3A and Supplementary Figure S3A). IAA treatment, however, resulted in a release of PID-VENUS from the PM to the cytoplasm within 5 minutes, and PM localization was restored 10 minutes after IAA addition (Supplementary Figure S3B-F). Pre-treatment of seedlings with  $LaCl_3$  did not influence PID localization by itself (Supplementary Figure S3G), but did inhibit IAA-induced dissociation of PID-VENUS from the PM (Supplementary Figure S3H). In contrast to protoplasts, the IAA induced dissociation of PID-VENUS from the PM in root epidermis cells occurred only transiently. As it has been experimentally established that IAA is very unstable under tissue culture conditions (Paciorek et al., 2005; Korasick et al., 2013), and the stable auxin analog naphthalene-1-acetic acid (NAA) was used in protoplast experiments, we repeated the treatments of *PID::PID-VENUS* roots with NAA. Like with IAA, PID internalization was observed after 5 minutes of NAA treatment (Figure 3B and Supplementary Figure S3I-L). This time, however, PID localization at the PM was not restored, and the kinase remained internalized after prolonged treatment (Figure 3C, D). Quantification showed that PID internalization gradually became stronger in time (Figure 3M). This data indicated that the restoration of PM localization after IAA treatment was due to IAA instability. Pre-treatment of seedlings with  $LaCl_3$  again inhibited NAA-induced dissociation of PID from the PM (Figures 3F-H, M), confirming that also the NAA-triggered response is dependent on the activity of PM-localized  $Ca^{2+}$  channels.

To analyze the involvement of TCH3 in auxin-triggered PID internalization, we selected the *Arabidopsis tch3-3* allele, with a T-DNA insertion at position -71 of the *TCH3* gene. This allele, was reported to be a complete loss-of-function mutant, based on Northern- and Western blot analysis (J. Braam, pers. com.), but did not display any obvious phenotypes, suggesting that TCH3 is functionally redundant with other CML proteins (McCormack and Braam, 2003). In the *tch3-3* background, NAA-induced PID-VENUS internalization was delayed but not abolished (Figure 3M).

These data corroborated our hypothesis that, like in protoplasts, auxin-triggered PM

dissociation of PID occurs in root epidermis cells, and that this response involves  $\text{LaCl}_3$ -sensitive  $\text{Ca}^{2+}$  channels and the  $\text{Ca}^{2+}$ -dependent binding of TCH3 or other redundantly acting CaMs or CMLs.

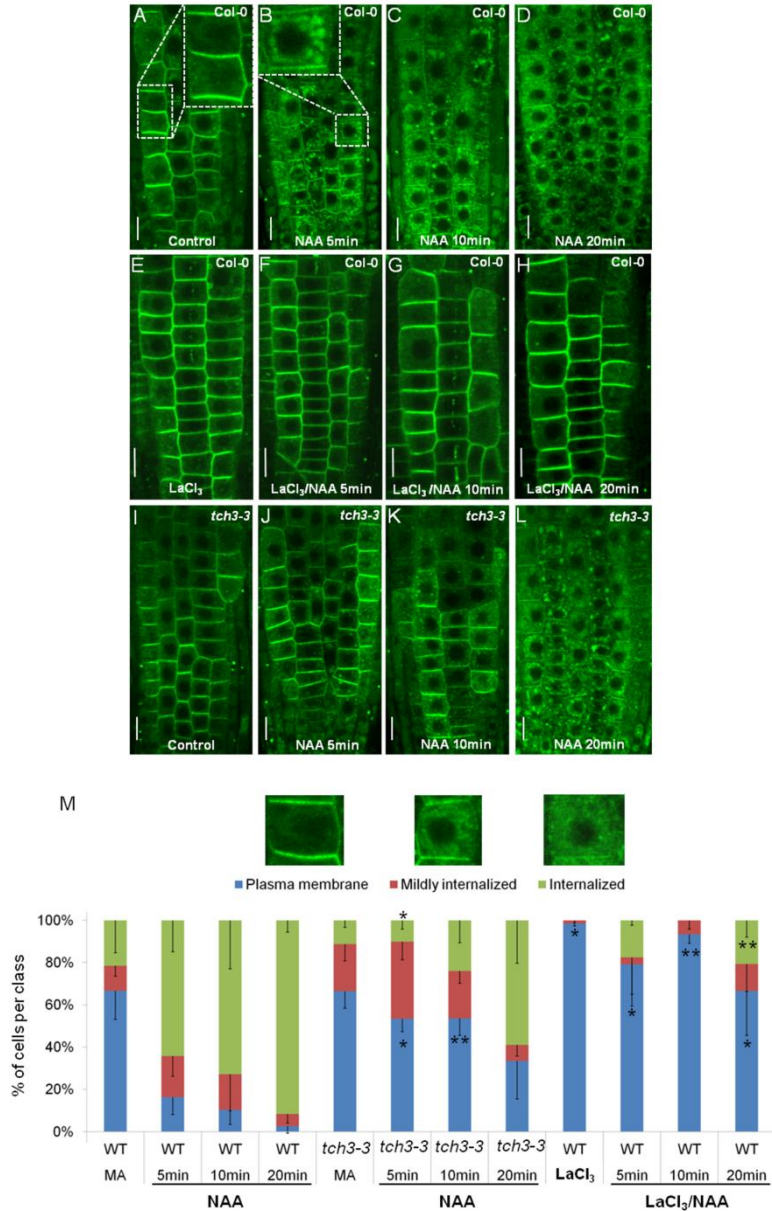


**Figure 3** Auxin-induced internalization of PID:VENUS in *Arabidopsis* root epidermis cells is  $\text{Ca}^{2+}$ - and

**TCH3-dependent.**

(A-L) Auxin treatment (5  $\mu$ M NAA) induces rapid internalization of PID-VENUS in *Arabidopsis* root epidermis cells of four days-old seedlings (A-D), but not after 30 minutes pre-treatment with 1.25 mM of the  $\text{Ca}^{2+}$  channel blocker  $\text{LaCl}_3$  (E-H). Auxin-induced PID-VENUS internalization is delayed in the *tch3-3* mutant background (I-L). Scale bars represent 10  $\mu$ m.

(M) Quantification of the results exemplified in A-L as percentage of cells displaying PM (mainly PM-localized PID, blue), mildly internalized (still some PM-localized PID visible, red), or completely internalized (no visible PM-localized PID, green) PID-VENUS signal in wild-type or *tch3-3* mutant seedlings. Values are based on 125 to 335 root epidermal cells in 4 to 9 seedlings. MA = MA medium (untreated). Error bars represent standard error of the mean. Asterisks indicate values from *tch3-3* and  $\text{LaCl}_3$ -treated seedlings that are significantly different from WT at the same time point: \* $p < 0.05$ ; \*\* $p < 0.01$  (*t*-test).

***TCH3* expression affects PID activity by reducing its PM localization**

In contrast to the *tch3-3* loss-of-function mutant, which did not show obvious phenotypes, *35S::TCH3* overexpression seedlings showed a significant reduction in root length (Figure 4A, B). The *pidwag1wag2* triple loss-of-function mutant also showed a reduced root length (Dhonukshe et al., 2010), and this together with the observed negative effect of TCH3 on the *in vitro* activity of PID (Figure 1A) suggested that *TCH3* overexpression resulted in reduced AGC3 kinase activity. To test this, we combined *TCH3* overexpression with the *PID::PID-VENUS* reporter or with *PID* overexpression. PID-VENUS showed a significantly increased internalization in the *TCH3* overexpression background compared to wild-type. Even without any auxin treatment, only 5% (39/758) of the *TCH3* overexpressing cells showed PM-localized PID-VENUS, whereas this was 69% (546/790) in wild-type cells (Figure 4C). In the strong *35S::PID-21* line, a basal-to-apical PIN polarity switch triggers a reduction in the root tip auxin maximum, causing the main root meristem to differentiate and collapse (Benjamins et al., 2001; Friml et al., 2004). This phenotype is observed in only 5% of the seedlings at 3 days after germination (DAG), but occurs in up to 97% of the seedlings at 6 DAG (Figure 4D). Overexpression of *TCH3* significantly reduced the *PID* overexpression-induced root meristem collapse (Figure 4D) from 75% to 31% at 4 DAG (Student's *t*-test,  $p < 0.05$ ) and from 97% to 81% at 6 DAG (Student's *t*-test,  $p = 0.06$ ). The levels of *PID* and *TCH3* expression were more or less comparable in 5 days old *35S::PID-21*, *35S::TCH3-4*, or *35S::PID-21/35S::TCH3-4* seedlings (Figure 4D). These observations corroborate the proposed role of TCH3 as negative regulator of

PID kinase activity (above, and (Benjamins et al., 2003)), and make it tempting to speculate that the delay in the *35S::PID-21* root meristem collapse in the *TCH3* overexpression background would be due to TCH3 binding, leading to inhibition of PID kinase activity and strong PID internalization away from its phosphorylation targets.

Previously we have shown that the *PID* overexpression induced root collapse could be rescued by genetic backgrounds or treatments that increased the auxin maximum in the root tip (Benjamins et al., 2001). For *TCH3* overexpression seedlings we found that the auxin maximum in the root tip was enhanced, as visualized by the enhanced expression of the *DR5::GFP* reporter in the columella root cap (Figure 4E) and the reduced expression of the *35S::DII-VENUS* reporter in the root epidermis (Figure 4G). This explains the reduced root length of *TCH3* overexpression seedlings (Figure 4B) as well as the delay in *PID* overexpression-induced root meristem collapse observed in the *35S::TCH3* background (Figure 4D).

The enhanced auxin maximum in *35S::TCH3-2* roots pointed toward changes in PIN polarity, especially in epidermis cells of the root tip where constitutive PID internalization was observed (Figure 4C). In these cells, PID partially colocalizes with PIN2 at the apical PM (Michniewicz et al., 2007), and PID-mediated phosphorylation of the PIN2 hydrophilic loop (PIN2HL) is required for apical PIN2 localization in the distal epidermis- and lateral root cap cells (Dhonukshe et al., 2010). In *35S::TCH3-2* root epidermis cells, PIN2-GFP showed increased localization to the lateral membranes compared to wild-type roots, as demonstrated by a significant decrease of the apical/lateral PIN2-GFP ratio in the *TCH3* overexpression background (Figures 4F).

Previously we showed that *in vitro* binding of TCH3 to PID is  $\text{Ca}^{2+}$  dependent (Benjamins et al., 2003), which is in line with the observed  $\text{Ca}^{2+}$ - and TCH3-dependency on auxin-induced PID internalization in the wild type background. However, the enhanced PID internalization observed in the *TCH3* overexpression background occurs in the absence of exogenous auxin, suggesting that the sensitivity of PID for  $\text{Ca}^{2+}$ -dependent internalization is regulated by the *TCH3* expression levels, and thus by the TCH3 protein abundance.

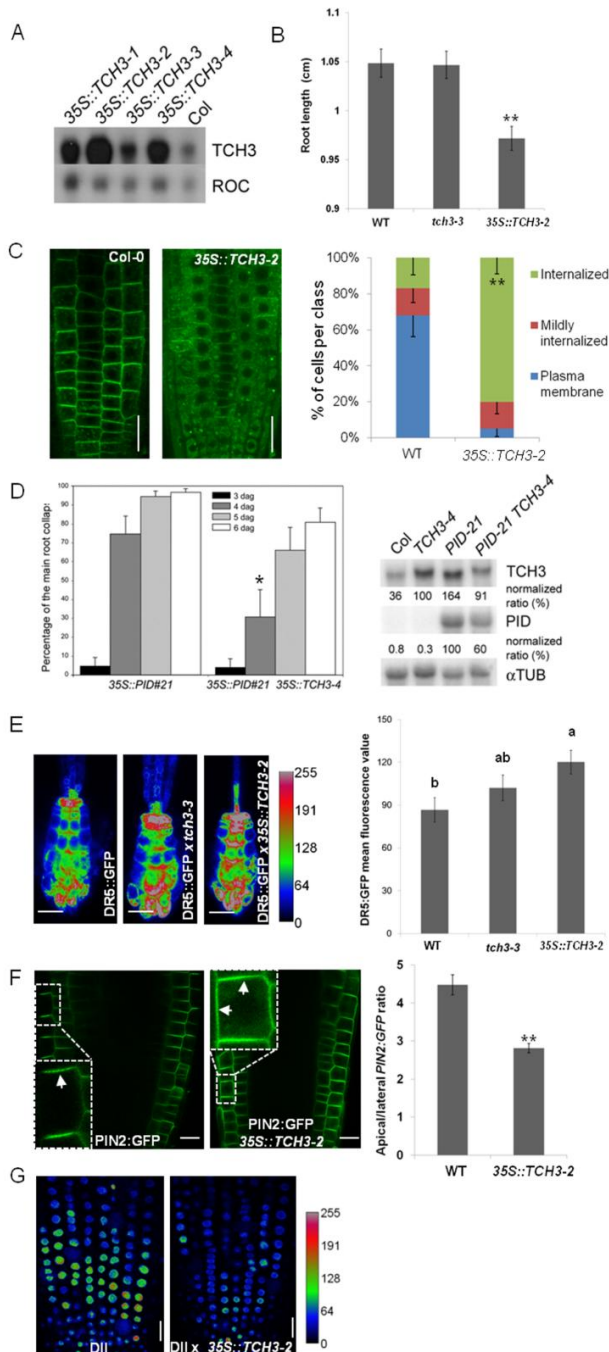


Figure 4 *TCH3* overexpression reduces PID PM localization and activity.

(A) Northern blot analysis showing the level of *TCH3* overexpression in four independent *35S::TCH3* lines (top). Hybridization with the *ROC* cDNA was used as loading control (bottom).

(B) Roots of 5-days old *35S::TCH3-2* seedlings are significantly shorter than those of wild-type (WT) and *tch3-3* seedlings (n=108 - 120).

(C) Confocal images (left, size bar indicates 10  $\mu$ m) and quantification of these images (right panel) showing PID-VENUS internalization in root epidermis cells (n=790 and 758, respectively) of 15 *PID::PID-VENUS* or *35S::TCH3-2/PID::PID-VENUS* roots. Internalization is expressed as percentage of cells displaying PM (blue), mildly internalized (red), or completely internalized (green) PID-VENUS signal.

(D) *PID* overexpression-induced collapse of the main root meristem is significantly delayed in the *35S::TCH3-4* background (left panel). Northern blot analysis shows the expression level of *TCH3* (top), *PID* (middle) and  $\alpha$ -*Tubulin* (bottom) in seedlings of the lines used in (left panel). The same blot was successively hybridized with the *PID*, *TCH3* or  $\alpha$ -*Tubulin* cDNA as probe. Intensities were quantified using ImageQuant and normalized to the corresponding  $\alpha$ -*Tubulin* sample to compensate for loading differences. The sample with *TCH3* or *PID* overexpression alone was put at 100%.

(E) *DR5::GFP* signal in WT, *tch3-3* and *35S::TCH3-2* root columella cells (images on the left), and quantification of these GFP signals (graph on the right). The significantly different classes are indicated with a to b (p<0.05, *t* test). The *DR5::GFP* signal intensity is color-coded (from blue to red indicates low to high expression).

(F) Confocal images of PIN2-GFP localization in WT and *35S::TCH3-2* root epidermis cells (images on the left). Quantification of the apical/lateral PIN2-GFP ratio (graph on the right, the mean fluorescence intensity of apical versus outer lateral membrane) shows that PIN2-GFP is significantly more apolar in the *35S::TCH3-2* background.

(G) *35S::DII-Venus* signal in WT (left) and *35S::TCH3-2* root tip epidermis cells (right).

Error bars in B, C, E and G represent the standard error of the mean, and significant differences are indicated with asterisks: \*p<0.05; \*\*p<0.01 (*t* test). The *DII-Venus* signal intensity is color-coded (from blue to red indicates low to high expression).

## Ca<sup>2+</sup> acts downstream of auxin during root gravitropism

It is well-established that root gravitropic growth is mediated by the PIN-driven asymmetric distribution of auxin over the root tip, resulting in differential elongation of cells at the upper and lower site of the root (Friml et al., 2002; Friml, 2003; Tanaka et al., 2006). At the same time, Ca<sup>2+</sup> signaling has been reported to be important during root gravitropism (Poovaiah et al., 1987; Roux and Serlin, 1987). Concentration peaks of cytoplasmic Ca<sup>2+</sup> have been found to coincide with the basipetal movement of auxin at the lower side of the root from the root tip toward the elongation zone, and auxin

treatment was shown to trigger a rise in cytosolic  $\text{Ca}^{2+}$  within seconds, indicating that  $\text{Ca}^{2+}$  acts downstream of auxin (Monshausen et al., 2011). Despite these investigations, however, it is still unclear whether  $\text{Ca}^{2+}$  only acts downstream of auxin, especially since  $\text{Ca}^{2+}$  signaling in the columella root cap has been suggested to be important for the onset of root gravitropism (Moore, 1985; Poovaiah et al., 1987). To investigate the timing of  $\text{Ca}^{2+}$ - and auxin signaling during the root gravitropic response, we gravity-stimulated roots in the presence of the  $\text{Ca}^{2+}$  channel inhibitor  $\text{LaCl}_3$  or the PAT inhibitor NPA. Global application of 1.25 mM  $\text{LaCl}_3$  blocked the root gravitropic response (Figure 5G), but not the *DR5::GFP* (Ottenschlager et al., 2003) or *35S::DII-VENUS* (Brunoud et al., 2012) reported asymmetric auxin distribution (Figure 5B, 5D, Supplementary Figure S4). In contrast, global application of 10  $\mu\text{M}$  NPA blocked gravity response (Figure 5H), as well as the establishment of an asymmetric *DR5::GFP* signal after gravity-stimulation (Figure 5C, D). These two experiments indicate that  $\text{Ca}^{2+}$  acts downstream of auxin redistribution during root gravitropism. Quantification of the asymmetric *DR5* signal 5.5 hours after gravistimulation showed that the intensity of the signal at the lower side of  $\text{LaCl}_3$  treated root tips was reduced compared to untreated root tips (Figure 5E). This indicates that PIN-dependent auxin transport might be impaired in  $\text{LaCl}_3$ -treated gravity-stimulated seedling roots. Because 1.25 mM  $\text{LaCl}_3$  might affect root gravitropism due to its inhibitory effect on root growth (Figure 5K), we performed the same tests on seedlings grown on a lower concentration (0.63 mM) that did not perturb root growth (Figure 5K), but did significantly delay gravity-dependent root bending (Figure 5I and J). From the effects of the drug treatments on the auxin response reporters and the root growth response we concluded that  $\text{Ca}^{2+}$  signaling is needed in the root gravitropic response, downstream of the asymmetric auxin redistribution, to maximize the asymmetric auxin response in the root tip, and thereby the speed of root bending.

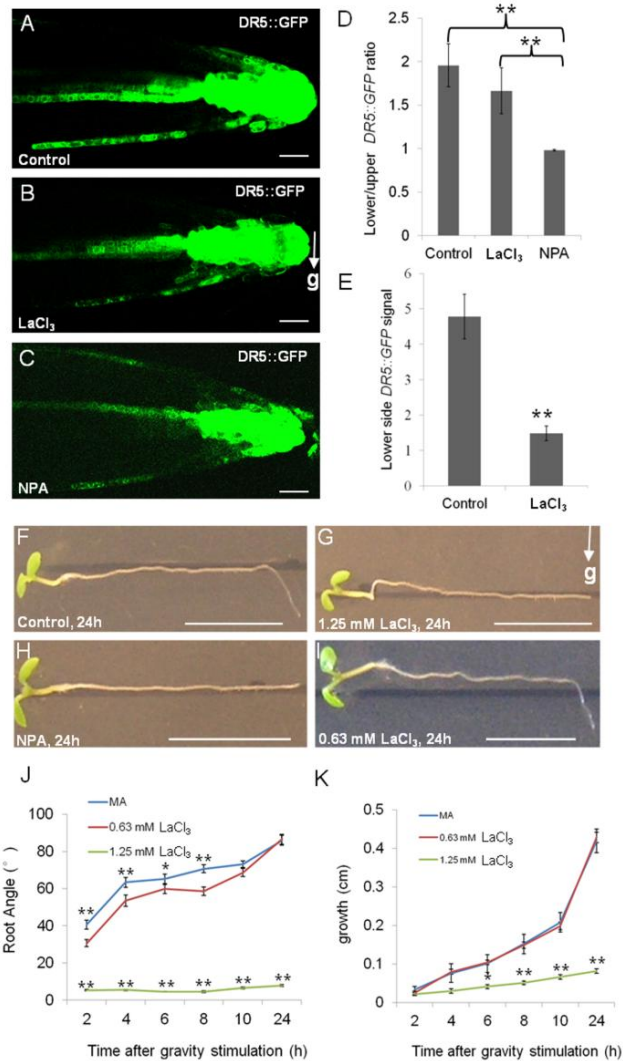


**Figure 5** Ca<sup>2+</sup> acts downstream of PIN-driven differential auxin responses during gravitropic root growth.

(A-E) Auxin response in *Arabidopsis* root tips 5.5 hours after gravity-stimulation, as indicated by the auxin responsive *DR5::GFP* reporter. Both untreated (A, D) and 1.25 mM LaCl<sub>3</sub> treated (B, D) roots show a clear asymmetric auxin response, whereas blocking polar auxin transport (10 μM NPA) results in a symmetric response (C, D). The mean intensity per pixel of the *DR5::GFP* signal at the lower side of LaCl<sub>3</sub>-treated root tips is significantly reduced compared to untreated gravistimulated control roots (E).

(F-I) Growth response of 5-days old seedling roots after 24 hours gravistimulation, on control medium (F), or

medium with 1.25 mM LaCl<sub>3</sub> (G), 10 μM NPA (H) or 0.63 mM LaCl<sub>3</sub> (I).

(J) Quantification of the gravitropic response of roots of 5-days old *Arabidopsis* seedlings on MA medium without or with 0.63 mM or 1.25 mM LaCl<sub>3</sub>.

(K) Quantification of the root growth (in cm) of seedlings in J from the start of the experiment.

Error bars in D, E, J and K represent the standard error of the mean, and significant differences are indicated with asterisks: \**p*<0.05; \*\**p*<0.01 (*t*-test). A white arrow (g) in B and G indicates the gravity direction. Scale bars in A to C = 20 μm. Scale bars in F to I = 0.5 cm.

### ***TCH3*-mediated control of PIN2 polarity maximizes the root gravitropic response**

In order for the auxin-induced Ca<sup>2+</sup> signaling in the epidermis cells at the lower side of the root to have an effect on the root gravitropic response, the Ca<sup>2+</sup> transients need to be translated by Ca<sup>2+</sup> sensors, such as TCH3. Both *tch3-3* loss-of-function and *35S::TCH3-2* gain-of-function seedlings showed a delay in root bending upon gravity-stimulation (Figure 6A), indicating a role for TCH3 in root gravitropism, and also suggesting that asymmetric expression of *TCH3* is important. Indeed, *TCH3::TCH3-GUS* seedlings showed asymmetric GUS staining at the lower side of root tips after 2-6 hours of gravistimulation (Figure 6B), which corresponds to the timing of the asymmetric auxin response in gravity stimulated root tips (Band et al., 2012), and is in line with *TCH3* being an auxin responsive gene (Antosiewicz et al., 1995; Benjamins et al., 2003). The reduced gravitropic response correlated with a significantly reduced lower/upper *DR5::GFP* ratio in *tch3-3* root tips (1.25) compared to that in wild-type (1.60) (Figure 6C). This again confirmed a role for TCH3 in optimizing root gravitropism by maximizing the differential auxin response in the root tip. In line with the previously observed enhanced auxin response in *35S::TCH3-2* root epidermis cells (Figure 4G), the mean lower/upper *DR5* ratio of gravity stimulated *35S::TCH3-2* root tips was slightly reduced, but the difference with wild-type roots was not significant (Figure 6C).

The clear involvement of TCH3 in root gravitropism suggested that auxin-induced TCH3-mediated PID internalization forms an integral part of the root gravitropic response. Indeed, when root tips of *PID::PID-VENUS* seedlings were gravity stimulated for 3 hours, PID-VENUS showed enhanced internalization in epidermis cells at the lower side of the root tip, whereas the kinase still showed predominant PM localization in epidermis cells at the upper side of root tip (Figure 6D). In roots incubated on medium supplemented with LaCl<sub>3</sub>, no enhanced PID internalization was observed

following gravistimulation (Figure 6D), confirming that auxin-triggered  $Ca^{2+}$  signaling is required for PID internalization.

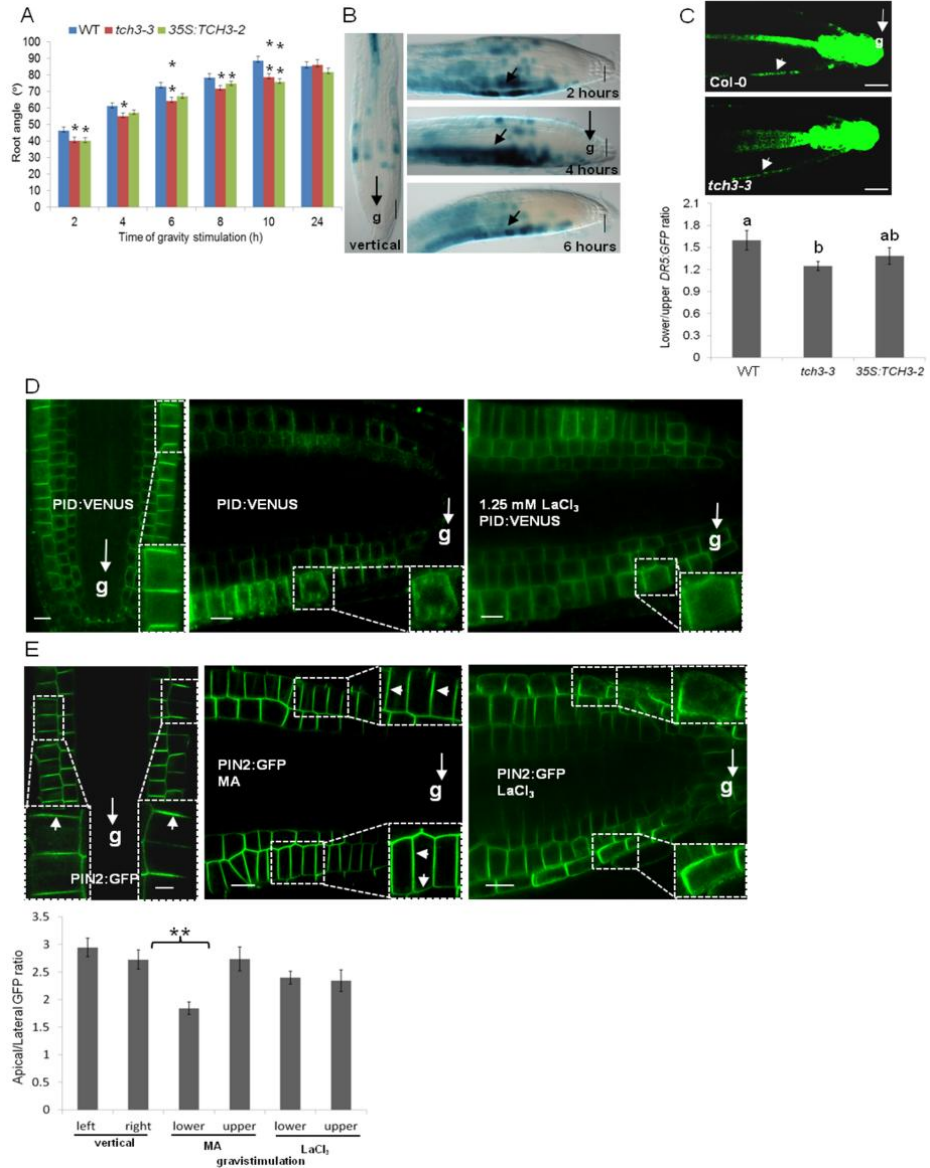


**Figure 6** TCH3-mediated PID internalization and PIN2 depolarization maximizes the root gravitropic response.

(A) Five-days old *tch3-3* loss-of-function mutant and *35S::TCH3-2* overexpression seedlings show a delayed root gravitropic response compared to wild-type (WT) seedlings.

(B) DIC images of GUS stained root tips of vertically grown *TCH3::TCH3-GUS* seedlings, or at 2, 4, or 6 hours after gravistimulation. Positions of enhanced GUS expression are marked by white arrows.

(C) Confocal images of root tips of five-days old *DR5::GFP* (WT) and *tch3-3/DR5::GFP* seedlings at 5.5 hours after gravistimulation. The graph shows the the ratio of the *DR5::GFP* signal in the upper and lower lateral root cap cells of wild-type (WT), *tch3-3* and *35S::TCH3-2* roots.

(D) In root epidermis cells of four-days old vertically grown *PID::PID-VENUS* seedlings, PID-VENUS is predominantly PM-localized (left image). Three hours of gravistimulation induces dissociation of PID-VENUS from the PM in cells at the lower side of the root tip (middle image), and this is inhibited by 1.25 mM  $\text{LaCl}_3$  (right image).

(E) At 3.5-5 hours after gravistimulation, the polarity of PIN2-GFP (*PIN2::PIN2-GFP*) in the lower epidermis cells shifts from predominantly apical (rootward) in untreated root tips (left image and graph) to a more apolar localization in gravistimulated root tips (middle image and graph).  $\text{LaCl}_3$  treatment prevents PIN2 apolarization (right image and graph). MA indicates MA medium without  $\text{LaCl}_3$ .

A white arrow (g) in B, C, D and E indicates the gravity direction. Arrow heads in E mark PIN2-GFP polarity. Scale bars indicate 20  $\mu\text{m}$  in B and C, and 10  $\mu\text{m}$  in D and E. Error bars in A, C and E represent the standard error of the mean, and significant differences in A and E are indicated with asterisks: \* $p < 0.05$ ; \*\* $p < 0.01$  (*t*-test). Significantly different values in the graph in C are classified with a and b ( $p < 0.05$ , *t*-test).

As was shown for *TCH3* overexpression roots (Figure 4G), we expected the enhanced PID internalization at the lower side of the gravity stimulated roots to lead to PIN2 depolarization. Indeed, PIN2-GFP showed a reduced apical-lateral polarity ratio in epidermis cells at the lower side of roots 3.5 hours after gravistimulation, whereas in epidermis cells at the upper side of the root this ratio was comparable to that in epidermis cells of unstimulated roots (Figure 6E). No significant difference in the apical-lateral PIN2 ratio between the upper side and lower side of gravistimulated root tips was observed after  $\text{LaCl}_3$  treatment (Figure 6E).

In conclusion, upon gravistimulation, auxin accumulation in the lower root epidermal cells induces PID internalization, by the increase in *TCH3* expression and at the same time by enhancing the TCH3-PID interaction through an increase in cytosolic

$\text{Ca}^{2+}$ . This internalization leads to PIN2 apolarity, which is necessary to maximize the auxin response at the lower side of the root tip. This is in line with the observation that inhibition of  $\text{Ca}^{2+}$  influx leads to a reduced differential auxin response (Figure 5B, E), whereas kinase loss-of-function or PIN2 loss-of-phosphorylation leads to an increased auxin response in the lateral root cap (Dhonukshe et al., 2010).

## Discussion

$\text{Ca}^{2+}$  is a common second messenger in signaling pathways, and has been found as one of the early signals in response to the plant hormone auxin. Experiments on plant cells have shown that the  $[\text{Ca}^{2+}]_{\text{cyt}}$  is increased within a few minutes after auxin application (Felle, 1988; Gehring et al., 1990b; Shishova and Lindberg, 2004; Monshausen et al., 2011). Furthermore,  $\text{Ca}^{2+}$  has also been reported as an important second messenger in the regulation of PAT (dela Fuente and Leopold, 1973). Here we investigated a previously identified molecular link between  $\text{Ca}^{2+}$  and the regulation of PAT, being the interaction of the CML TCH3 with the PID kinase (Benjamins et al., 2003). Surprisingly, our research uncovered a new role for the  $\text{Ca}^{2+}$ -dependent binding of CaM/CML to substrate proteins, being the recruitment of a PM-associated kinase from the PM to the cytosol, away from its PIN phosphorylation targets. Our results further clarify the molecular link between  $\text{Ca}^{2+}$  signaling and auxin transport, and suggest that beside its role in optimizing the root gravitropic response through regulation of PIN2 localization and auxin redistribution, the CML-kinase complex might be a generic signaling route through which auxin or other (environmental) signals that trigger a  $\text{Ca}^{2+}$  response can modulate PAT.

### **$\text{Ca}^{2+}$ /calmodulin-regulated PM association: a novel mechanism to regulate kinase activity**

Previously, we used *in vitro* pull down assays to show that TCH3 interacts with PID in a  $\text{Ca}^{2+}$ -dependent manner (Benjamins et al., 2003). Here, a similar assay was used in combination with PID deletion constructs to show that TCH3 interacts with the PID catalytic domain. Moreover, co-expression of TCH3-YFP and PID-CFP in *Arabidopsis* protoplasts and subsequent FRET measurements demonstrated the *in vivo* interaction between the two proteins, and showed that TCH3-YFP sequesters the active PM-associated PID-CFP kinase fusion protein to the cytoplasm. This suggests that interaction between TCH3 and PID provokes the release of the kinase from the PM. This sequestration of PID is auxin-dependent, as auxin-starved protoplasts do not show

internalization of PID. In addition, in root epidermis cells we observed that minutes after auxin treatment PID-VENUS is sequestered from the PM to the cytosol. Our data indicate that TCH3 is at least partially responsible for this process, and that most likely other CaMs/CMLs act redundantly with TCH3. As in the protoplast system, treatment with the auxin analog NAA resulted in rapid and more long term cytosolic localization of PID-VENUS (within 5 minutes for up to at least 1 hour), whereas, PM localisation of PID-VENUS was restored after 20 minutes when the natural auxin IAA was used. Previously, it was shown that the natural auxin is unstable in tissue culture, and is rapidly turned over, whereas NAA is not (Paciorek et al., 2005), and this is likely to explain the difference observed. In fact, a very transient increase in  $[Ca^{2+}]_{cyt}$  (from few to 60 seconds, with a peak around 30 seconds) was detected in *Arabidopsis* root epidermis cell after application of 100 nM IAA (Monshausen et al., 2011), whereas the NAA-induced increase in  $[Ca^{2+}]_{cyt}$  in wheat protoplasts lasted for at least 500 seconds (Shishova and Lindberg, 2004; Shishova et al., 2007). As long term elevation of  $[Ca^{2+}]_{cyt}$  is toxic to cells (Swanson et al., 2011), the prolonged auxin-induced internalization of PID might be achieved by two parallel mechanisms: the rapid internalization is achieved by a rapid increase in  $[Ca^{2+}]_{cyt}$ , after which the internalization is maintained by auxin-induced *TCH3* expression, which enhances the sensitivity of the system to  $Ca^{2+}$ , thereby lowering the  $[Ca^{2+}]_{cyt}$  required for prolonged PID internalization to sub-lethal levels. The observed oscillations in  $[Ca^{2+}]_{cyt}$  might further reduce the toxicity of  $Ca^{2+}$  in the cytosol (Shishova and Lindberg, 2004; Shishova et al., 2007). During root gravitropism, PID internalization can only be observed several hours after the start of gravistimulation. Since the peak in  $[Ca^{2+}]_{cyt}$  is already observed 6 minutes after gravistimulation, followed by moderately elevated  $[Ca^{2+}]_{cyt}$  (Monshausen et al., 2011), PID internalization probably requires the induction of *TCH3* expression by auxin.

Data by Zegzouti and co-workers indicate that PID binds to phosphorylated inositides and phosphatidic acid, and that a specific amino acid sequence inside the PID catalytic domain (insertion domain) is the key determinant for its membrane association (Zegzouti et al., 2006). We therefore hypothesize that PID co-localizes at the PM with its phosphorylation targets, the PIN auxin efflux carriers (Michniewicz et al., 2007), through the interaction of the insertion domain with membrane components. An increase in  $[Ca^{2+}]_{cyt}$ , e.g. induced by auxin, facilitates binding of TCH3 to the catalytic domain of PID, thereby preventing the kinase-lipid interaction and resulting in sequestration of the kinase away from its phospho-targets to the cytoplasm (Figure 7A).

Based on this model, it would be interesting to test whether TCH3 and phosphoinositides are competing for the interaction with the PID catalytic domain.

PKC, one of the animal orthologs of the plant specific AGCVIII kinases to which PID belongs (Galván-Ampudia and Offringa, 2007; Rademacher and Offringa, 2012), directly binds  $\text{Ca}^{2+}$  through a C2 domain.  $\text{Ca}^{2+}$  binding to this domain promotes a change in PKC subcellular localization from cytosol to PM and enhances affinity of the C2 domain for phosphorylated inositides (Corbalan-Garcia et al., 2007). This PM translocation activates the PKC kinase. PID is also thought to be active at the PM. However, in this case, the (auxin-induced) increase in  $[\text{Ca}^{2+}]_{\text{cyt}}$  results in the opposite effect and removes the kinase from the PM. PID does not have typical  $\text{Ca}^{2+}$  binding domains, and instead the kinase interacts in a  $\text{Ca}^{2+}$ -dependent manner with the  $\text{Ca}^{2+}$  receptor TCH3. An analogous system exists in animal cells, where a CaM competes with PM localized phosphatidylinositol 4,5 bisphosphate ( $\text{PIP}_2$ ) for binding to a cluster of basic amino acid residues in peripheral- or transmembrane proteins, thereby pulling the cluster from the PM. In animal cells this system is used to regulate the levels of free  $\text{PIP}_2$ , or the activity of transmembrane receptors (McLaughlin and Murray, 2005). To our knowledge, the  $\text{Ca}^{2+}$ - and CaM-dependent release of the PID kinase from the PM is a new form of regulating the activity of a kinase that is designed to phosphorylate PM proteins.

### **TOUCHing PID: a regulatory loop that translates cellular $\text{Ca}^{2+}$ levels to PIN polarity**

Our findings on TCH3-mediated PID internalization can be integrated into the current *Arabidopsis*-based model for gravitropic root growth (Band et al., 2012; Baster et al., 2013). Gravistimulation of roots leads to rapid lateral relocation of PIN3 and PIN7 to the lower side of columella root cap cells (Friml et al., 2002; Kleine-Vehn et al., 2010), resulting in auxin transport from the auxin maximum at the root tip to the lateral root cap- and epidermis cells at the lower side of the root tip (Figure 7B: 5 minutes) (Band et al., 2012; Brunoud et al., 2012; Baster et al., 2013). The higher auxin levels in these cells lead to stabilization of PIN2 at the PM by inhibition of ABP1-mediated endocytosis, whereas PIN2 is degraded due to reduced auxin levels at the upper side of the root tip (Figure 7B: between 5 and 90 minutes) (Paciorek et al., 2005; Abas et al., 2006; Robert et al., 2010; Baster et al., 2013). The enhanced auxin levels at the lower side of the root tip also lead to a rapid increase in  $[\text{Ca}^{2+}]_{\text{cyt}}$  and to an induction of *TCH3* expression (Antosiewicz et al., 1995; Monshausen et al., 2011). The elevated TCH3

levels together with the higher  $[Ca^{2+}]_{\text{cyt}}$  result in sequestration of PID from the PM to the cytosol (Figure 7 A and B: between 1,5 to 5 hours). Consequently, a reduction of PM-associated PID levels eventually results in PIN2 apolar localization at the lower side of root tip, leading to enhancement of the asymmetric auxin distribution (Figure 7B: between 1.5-5 hours). This proposed model implies that a  $Ca^{2+}$  release negatively and transiently regulates PID activity through its TCH3-induced dissociation from the PM, away from its PIN phosphorylation-targets. The TCH3-dependent inactivation of PID may be part of a regulatory loop that allows fast and possibly subtle alterations in PIN polarity in response to signals that lead to rapid changes in cytosolic  $Ca^{2+}$  levels, such as auxin (Felle, 1988; Gehring et al., 1990b; Shishova and Lindberg, 2004) and unidirectional blue light or mechanical stress (Lee et al., 1984; Gehring et al., 1990b; Baum et al., 1999; Harada et al., 2003; Monshausen et al., 2009).

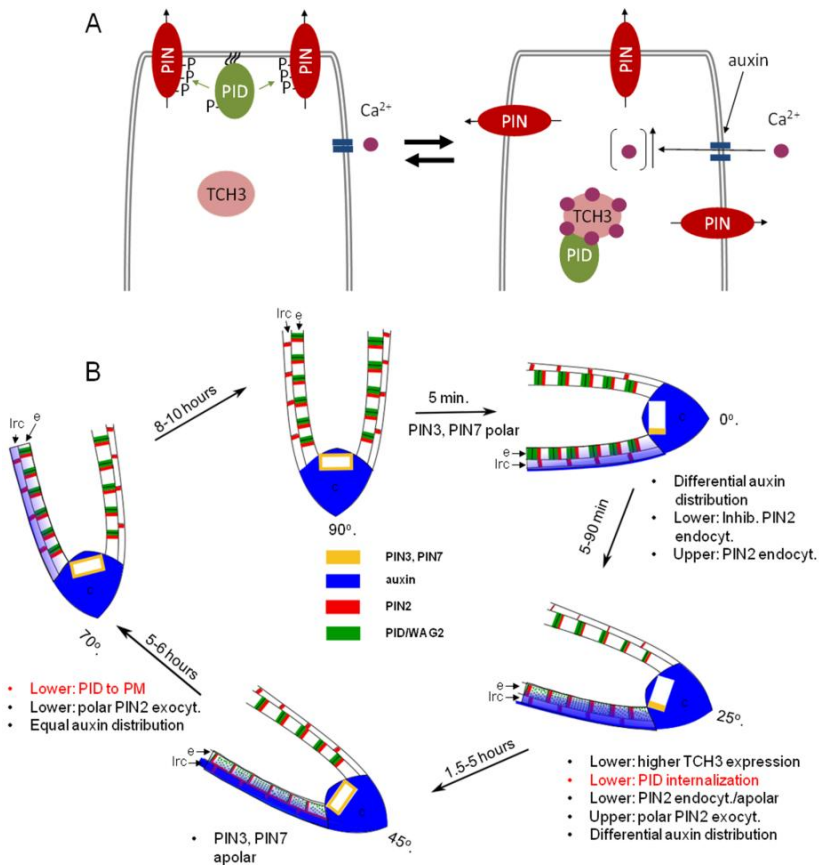


**Figure 7 TCH3-mediated PID sequestration and its role in auxin-directed PIN polarity regulation during root gravitropism**

(A) Model for auxin-induced sequestration of PID from the PM to the cytoplasm. Elevated auxin levels increase the  $[Ca^{2+}]_{\text{cyt}}$ , by activating PM-localized  $Ca^{2+}$  channels. Binding of  $Ca^{2+}$  to the EF-hands of the calmodulin-like protein TCH3 enhances its affinity for PID, whereby TCH3 is able to compete for PID binding to PM components. This leads to sequestration of PID from the PM to the cytosol, away from its PIN phosphorylation targets, resulting in PIN dephosphorylation and apolarity.

(B) Model for the involvement of TCH3-mediated PID and WAG2 sequestration in root gravitropism. In vertically oriented roots ( $90^\circ$ ), PIN3 (yellow) is symmetrically distributed at the PM of columella cells, resulting in a uniform distribution of auxin (blue) from the columella to the lateral root cap and epidermis, where PID and WAG2, localized mainly at apical (shootward) and basal (rootward) PM (green), maintain an apical flow of auxin by directing apical localization of PIN2 (Red). Minutes after gravistimulation, PIN3 relocates to the lower side of columella cells (5 min), redirecting the auxin stream, and resulting in stabilization of PIN2 at the PM and in an enhanced auxin response at the lower side of the gravistimulated root (5-90 minutes). This auxin response on the one hand triggers  $Ca^{2+}$  channels, and on the other hand induces *TCH3* expression, causing gradual PID internalization at the lower epidermis of the root tip. The resulting reduction in PIN2 phosphorylation induces PIN2 apolar localization, thereby reducing the apical auxin flow and enhancing the auxin response at the lower lateral root cap and epidermis of the root tip. This mechanism maximizes the gravitropic growth response (1.5 – 5 hours), and provides feed back to the asymmetric root growth, at a later time point (5-6 hours) by normalizing PIN localization and restoring the auxin distribution to that of a vertically growing root (8-10 hours). lrc: lateral root cap; e, epidermis; c: columella.

By *in vitro* pull down assays and co-expression in *Arabidopsis* protoplasts we showed that not only PID, but also WAG2 interacts with and is sequestered by TCH3 from the PM. In view of the expression of WAG2 in epidermis cells of the root tip, it is likely that the TCH3-WAG2 interaction plays a role in root gravitropism. No clear interaction was observed between TCH3 and WAG1 or AGC3-4, indicating that the AGC3 kinases do not function completely redundant, and also that the amino acid sequence requirement for the interaction with TCH3 is only present in two of the four AGC3 kinases. Auxin is known to regulate its own transport, firstly by inhibiting ABPI-dependent PIN endocytosis (Paciorek et al., 2005; Robert et al., 2010), and secondly by regulating E3 ubiquitin ligase SKP-Cullin-F-box<sup>TIR1/AFB</sup> (SCF<sup>TIR1/AFB</sup>)-dependent processes, such as canalization of the auxin flow in response to increased cellular auxin concentrations (Sauer et al., 2006), or enhanced PIN turnover

by sub-optimal auxin levels (Baster et al., 2013). Sauer and co-workers still observed PIN lateralization in auxin-treated *35S::PID* seedlings, suggesting that PID is not involved in this SCF<sup>TIR1/AFB</sup>-dependent process (Sauer et al., 2006). It will be interesting to test, however, whether the TCH3-mediated PID sequestration plays a role in SCF<sup>TIR1/AFB</sup>-dependent PIN turnover. This would imply that a reduction in PM-associated PID, besides PIN2 depolarization, would also lead to enhanced PIN degradation, thereby providing a mechanism to normalize PIN2 levels to the situation before gravistimulation. Our results suggest that elevated cellular auxin levels may transiently alter PID kinase activity by subcellular localization changes and inhibition of its kinase activity via the interaction with TCH3. This sets the stage for a different type of auxin-dependent PIN lateralization, and leads to a subtle modulation of PIN polar targeting, e.g during tropic growth responses.

In conclusion, we show that during gravitropism asymmetric auxin transport and subsequently Ca<sup>2+</sup> influx into epidermis cells at the lower side of the root tip stimulate TCH3-mediated sequestration of PID from the PM to the cytosol. As a consequence of PID inactivation PIN2 is dephosphorylated, causing apolar localization and possibly enhanced degradation of PIN2 at the lower side of the root tip. The reduced PAT results in enhanced auxin accumulation at this side. Hence accentuating the growth response mediated by the asymmetric auxin distribution (Figure 7).

### **Is ABP1 signaling involved in auxin-induced PID-TCH3 interaction?**

The auxin-induced interaction between PID (or WAG2) and TCH3 can be observed already 5 minutes after auxin treatment. This rapid response suggests that the required increase in Ca<sup>2+</sup> levels does not involve *de novo* gene transcription, but is rather mediated by rapid activation of Ca<sup>2+</sup> channels at the PM. The ABP1 auxin receptor is known to be secreted to the extracellular space where it regulates cell elongation and cell division (Steffens et al., 2001; David et al., 2007; Braun et al., 2008; Dahlke et al., 2010), and its action has been linked to the promotion of clathrin-mediated endocytosis (Robert et al., 2010). Recent data indicate that auxin-induced ABP1 signaling to downstream non-transcriptional responses requires its interaction with a small subfamily of four Trans Membrane receptor-like Kinases (TMKs) (Xu et al., 2014). Being the only known auxin receptor at the PM, ABP1 is a likely candidate for mediating the auxin effects on cytosolic Ca<sup>2+</sup> levels. We tested this possibility, by combining the *PID::PID-VENUS* reporter with the ethanol-inducible anti-ABP1 lines *SS12K9* and *SS12S6* or with the *abp1-5* allele containing a point mutation (His94->Tyr)

in the auxin-binding pocket that is predicted to reduce auxin binding affinity (Woo et al., 2002; Braun et al., 2008; Xu et al., 2010). Unfortunately, ethanol treatment already led to complete PID-internalization in wild-type background, which prevented the use of the SS12K9 and SS12S6 lines for these experiments (data not shown). Moreover, in the *abp1-5* background we did not observe a significant reduction in auxin-induced PID-VENUS internalization (data not shown), mostly because PID-VENUS was already more internalized in this background. Interestingly, the *abp1-5* mutant protein already shows some background interaction with TMK (Xu et al., 2014), suggesting that the observed enhanced PID-VENUS internalization is caused by a low level of constitutive TMK activation by the *abp1-5* protein. In view of the strong effects of complete loss-of-function *abp1* mutations (Chen et al., 2001), and the sensitivity of PID-VENUS for internalization, it might be difficult to show unequivocally whether or not ABP1 is involved in triggering the Ca<sup>2+</sup> signaling that leads to PID internalization.

## Experimental procedures

### Molecular cloning and constructs

Molecular cloning was performed following standard procedures (Sambrook, 1989). Bacteria were grown on LC medium containing 100 µg/ml carbenicillin (Cb, all high copy plasmids), 50 µg/ml kanamycin (Km, pGreen) or 250 µg/ml spectinomycin (Spc, pART 27) for *E.coli* strains DH5α or 20 µg/ml rifampicin (Rif) and 50 µg/ml Km, or 250 µg/ml Spc for *Agrobacterium* strain LBA1115 (Hood et al., 1993). The constructs *pSDM6008* (*pET16H:TCH3*), *pSDM6004* (*pGEX:PID*), *pSDM6005* (*pBluescript SK-PID*) and *pET16H:PBPI* were described previously (Benjamins et al., 2003). Primers used in this study are listed in Table 1. To obtain a plasmid encoding the GST-tagged first 100 amino acids of PID, the *Sall-SacI* (blunted) fragment from *pSDM6005* was cloned into the *XhoI* and *HindIII* (blunted) sites of *pGEX-KG* (Guan and Dixon, 1991). Fragments encoding the PID catalytic domain (aa 75-398) and the C-terminal part of PID (aa 339-438) were obtained by PCR amplification using the primer pairs PID PK CaD F-PID PK CaD R and PID PK CT F-PID PK CT R, respectively, and cloned into *pGEX-KG* using *XhoI-HindIII* (blunted) and *EcoRI-HindIII* (blunted), respectively.

Expression vectors *p35S::YFP* and *p35S::CFP* were obtained by inserting the *YFP-HA* and *FLAG-CFP* coding regions with appropriate restriction enzymes between the *CaMV 35S* promoter and the *CaMV 35S* terminator of *pART7*. Expression vectors *pGEX-PID*, *pGEX-WAG1*, *pGEX-WAG2*, *pGEX-AGC3-4*, *p35S::YFP-CFP*, *p35S::PID-CFP*, *p35S::WAG1-CFP*, *p35S::WAG2-CFP*, *p35S::AGC3-4-CFP*, *35S::TCH3-YFP* and *pET16H-PID* were constructed using the Gateway Technology (Invitrogen). BP reactions were performed in *pDONR207* according to manufacturer's instructions (Invitrogen). LR reactions were performed in either the pGEX-based destination vector for N terminal fusions with the Glutathione-S-transferase (GST), or the *pART7*-based destination vectors. The *pART7*-based destination vectors were obtained by inserting the recombination cassette in frame with the *YFP-HA*, *FLAG-CFP* or *mRFP1* coding region between the *CaMV 35S* promoter and the *CaMV 35S* terminator. The *pGEX*-based destination vector was obtained by inserting the recombination cassette in frame with the *GST* coding region. For the *pGreenII-0229mRFP* destination vector, the recombination cassette in frame with the *mRFP1* coding region was excised from the *pART7*-based destination vector and cloned into *pGreenII0229* (Hellens et al., 2000). The coding region of *YFP-HA* was amplified from *pART7 Gateway YFP-HA* using primer pair YFP attB F-YFP attB R. The coding regions of *PID* and *AGC3-4* were

amplified from *Arabidopsis thaliana* ecotype Columbia (Col-0) cDNA from siliques using respectively primer sets PID attB F-PID attB R, and AT2 attB F-AT2-Stop attB R. Coding regions for *WAG* genes were PCR amplified from *Arabidopsis thaliana* Col-0 genomic DNA using respectively primer sets WAG1 attB F-WAG1-Stop attB R, and WAG2 attB F-WAG2-Stop attB R.

**Table 1 Primer list. The attB recombination sites in the primer sequence are underlined.**

PID PK CaD F	5'TTC- <u>XhoI</u> -TTTCGCCTCAT3'
PID PK CaD R	5'GCGCTCAGTTTAGACCTTTGA3'
CT F	5'TAATGACG- <u>EcoRI</u> -TCCGTAACAT3'
CT R	5'AAGCTCGTTCAAAAAGTAATCGAAC3'
TCH3 attB F1	5'GGGG <u>ACAAGTTTGTACAAAAAGCAGGCTT</u> AATGGCGGATAAGCTCACT3'
TCH3 attB R1	5'GGGG <u>ACCACTTTGTACAAGAAAGCTGGGTA</u> AAGATAACAGCGCTTCGAACA3'
gTCH3 attB F	5'GGGGACAAGTTTGTACAAAAAGCAGGCTTAAAGACTCTTATAAGGACTC3'
gTCH3 attB R	5'GGGG <u>ACCACTTTGTACAAGAAAGCTGGGTA</u> AAGATAACAGCGCTTCGAACA3'
YFP attB F	5'GGGG <u>ACAAGTTTGTACAAAAAGCAGGCTT</u> CAGGGTGAGCAAGGGCGAGG3'
YFP attB R	5'GGGG <u>ACCACTTTGTACAAGAAAGCTGGGTCGATCCGGTGGATCCCGGGC</u> 3'
PID attB F1	5'GGGG <u>ACAAGTTTGTACAAAAAGCAGGCTT</u> CAGCATGTTACGAGAATCAGACGGT3'
PID attB R1	5'GGGG <u>ACCACTTTGTACAAGAAAGCTGGGTC</u> AAAAGTAATCGAACGCCGCTGG3'
PID exon1 F1	5'TCTCTCCGCCAGGTA AAAA3'
PID exon2 R1	5'CGCAAGACTCGTTGGAAAAG3'
TCH3pr F1	5'AAATGTCCACTCACCCATCC3'
TCH3pr R1	5'GGGAATTCTGAAGATCAGCTTTTGTTCG3'
LBaI	5'TGGTTCACGTAGTGGCCATCG3'
AtROC5 F	5'CGGGAAGGATCGTGATGGA3'
AtROC5 R	5'CCAACCTTCTCGATGGCCT3'
$\alpha$ TUB F	5'CGGAATTCATGAGAGAGATCCTTCATATC3'
$\alpha$ TUB R	5'CCCTCGAGTTAAGTCTCGTACTCCTCTTC3'
AT2 attB F	5'GGGG <u>ACAAGTTTGTACAAAAAGCAGGCTT</u> CAGCATGGCTAATTCTAGTATCTTT3'
AT2-Stop attB R	5'GGGG <u>ACCACTTTGTACAAGAAAGCTGGGTC</u> AAAATAATCAAATAATTAGA3'
WAG1 attB F	5'GGGG <u>ACAAGTTTGTACAAAAAGCAGGCTT</u> CAGCATGGAAGACGACGGTTATTAC3'

WAG1-Stop attB R	5'GGGG <u>ACCACTTTGTACAAGAAAGCTGGGTCTAGCTTTTTACCCACATAATG3'</u>
WAG2 attB F	5'GGGG <u>ACAAGTTTGTACAAAAAAGCAGGCTTAGGATGTGTTTGTGTCCCTTTGT3'</u>
WAG2-Stop attB R	5'GGGG <u>ACCACTTTGTACAAGAAAGCTGGGTCAACGCGTTTGC</u> ACTCGCGTA3'

To overexpress *TCH3* in *Arabidopsis thaliana*, its complete coding region was cloned from *pSDM6008* as a *Bam*HI fragment into *pART7* and the expression cassette was inserted as a *Not*I fragment into the *pART27* binary vector. To construct *35S::TCH3:YFP*, *35S::PID:CFP* and *pET16H:PID*, the coding regions were amplified by PCR from *pSDM6008* and *pSDM6004* with respectively primer pairs TCH3 attB F1-TCH3 attB R1, and PID attB F1 - PID attB R1 and the resulting PCR fragments were recombined into *pDONR207* (BP reaction) and subsequently into *pART7*-driven or *pET16H* destination vectors (LR reaction), containing either the *CFP* (PID), the *YFP* (TCH3) or His (PID) coding region in frame with the Gateway cassette (Invitrogen).

The binary vector *TCH3::TCH3-mRFP* was obtained by PCR amplification of a genomic fragment (from 1125 bp upstream until the stop codon) from *Arabidopsis thaliana* Col-0 genomic DNA using primer pairs gTCH3 attB F – gTCH3 attB R, recombining the resulting PCR fragment into *pDONR207* (BP reaction) and subsequently into the *pGreenII-0229-mRFP* destination vector (LR reaction). Design of cloning strategies, DNA sequence analysis and DNA and protein sequence alignments were performed using the Vector NTI 10 software (Invitrogen).

### **Arabidopsis lines, plant transformation and protoplast transfections**

*Arabidopsis* seeds were germinated and plants were grown as described (Benjamins et al., 2001). The lines *35S::PID-21* (Benjamins et al., 2001), *TCH3::TCH3-GUS* (Sistrunk et al., 1994), *PID::PID-VENUS* (Michniewicz et al., 2007), *DR5rev::GFP* (Benkova et al., 2003), *PIN2::PIN2-GFP* (Xu and Scheres, 2005), *abp1-5* (Xu et al., 2010) and *35S::DII-VENUS* (Brunoud et al., 2012) were described previously. *tch3-3* was kindly provided by J.Braam. For all experiments, *Arabidopsis thaliana* Col-0 ecotype was used as wild-type control.

Double loss- or gain-of-function lines were generated by crossing parental lines, and selected using either resistance markers or by genotyping. To genotype for the presence of the different T-DNA insertions, the T-DNA-specific LBa1 primer was combined in a PCR reaction with the gene-specific PCR primers TCH3pr F1 or TCH3pr R1 for *tch3-3*

(Table 1). Sequencing of the junction fragment was used to confirm the insertion position.

*Arabidopsis thaliana* ecotype Columbia wild type was transformed by the floral dip method as described (Clough and Bent, 1998) using *Agrobacterium* LBA1115 strain. T1 transformants were selected on medium supplemented with 50 µg/ml kanamycin (Km) for 35S::*TCH3*, with 30 µg/ml phosphinotricin (PPT) for *TCH3::TCH3-mRFP* and with 100 µg/ml timentin to inhibit the *Agrobacterium* growth. For further analysis, single locus insertion lines were selected by germination on 25 µg/ml Km or 15 µg/ml PPT.

Protoplasts were obtained from *Arabidopsis thaliana* Columbia cell suspension cultures that were propagated as described (Schirawski et al., 2000). Protoplast isolation and PEG-mediated transfections with 10 µg plasmid DNA were performed as described (Maraschin et al., 2009). To obtain auxin-starved protoplasts, auxin (NAA) was removed from the media during protoplast isolation. Following transfection, the protoplasts were incubated for at least 16h in the dark prior to observation.

### **Phenotypic and microscopy analysis**

For gravitropism experiments, plants were grown on vertically placed plates containing a 3-mm layer of MA medium (Masson and Paszkowski, 1992) solidified with 1% agar (Daichin). For gravistimulation, 5 days old seedlings were transferred to fresh medium, where indicated supplemented with LaCl<sub>3</sub> (125 mM stock in H<sub>2</sub>O; Sigma), or N-1-Naphthylphthalamic acid (NPA, 20 mM stock in DMSO; Pfaltz&Bauer). Roots were straightened and plates were incubated vertically and subsequently turned 90° to start the gravistimulation. Plates were imaged using a digital camera and root lengths and bending angles were measured with the Image J software (<http://rsb.info.nih.gov/ij/>).

For the root collapse assay, about 200 seedlings per line were grown in triplicate on vertical plates containing solid MA medium. During 8 days the seedlings were monitored and scored daily for collapse of the primary root meristem.

For β-glucuronidase (GUS) expression analysis, seeds of *TCH3::TCH3-GUS* were germinated for 5 days on solid MA medium, then transferred to liquid medium supplemented with 5 µM IAA (Indole-3-acetic acid, 8.6 mM stock in DMSO) or 5 µM NAA (1-Naphthylacetic acid, BDH, 10 mM stock in DMSO) for auxin induction or to MA medium and gravistimulated for 2, 4, 6 hours. Seedlings were stained for GUS activity as described (Benjamins et al., 2001) and analyzed and imaged using a Zeiss Axioplan II microscope with differential interference contrast (DIC) optics and camera.

For the subcellular localization of PID in *Arabidopsis* roots, vertically grown 4-days old *PID::PID-VENUS* seedlings were treated for 5, 10 or 20 minutes with 5  $\mu\text{M}$  IAA or NAA. For control treatments an equal amount of solvent (DMSO) was added to the medium. For pre-treatment with  $\text{Ca}^{2+}$  channel blocker, seedlings were incubated for 30 min on medium containing 1.25 mM  $\text{LaCl}_3$  (Sigma), after which the seedlings were transferred to medium with 1.25 mM  $\text{LaCl}_3$  together with 5  $\mu\text{M}$  IAA or NAA.

Confocal microscopy on *PID::PID-VENUS*, *PIN2::PIN2-GFP* and *TCH3::TCH3-mRFP* seedlings was done using the Zeiss LSM 5 Exciter 2C/1F Imager M1 (Zeiss, Oberkochen, Germany) confocal microscope, using a 40x oil objective. The YFP fluorescence was monitored with a 530-600 nm band pass emission filter (514 nm excitation). The GFP fluorescence was monitored with a 505-530 nm band pass emission filter (488 nm excitation). The RFP fluorescence was monitored with a 560 nm long pass filter (543 nm excitation). The images were analysed and processed in Image J (<http://rsb.info.nih.gov/ij/>) and assembled in Adobe Photoshop.

To quantify the ratios of PIN2-GFP between outer lateral and apical PM, signals were measured using median optical sections by drawing a freehand line in Image J, and calculating the mean fluorescence intensity per pixel. *DR5::GFP* and *35S::DII:Venus* signals were quantified after gravistimulation, by measuring the lower and upper fluorescent signals in freehand boxed lateral root cap cells using median optical sections in ImageJ. *DR5:GFP* signals in QC and columella cells were measured by freehand boxing the fluorescent signal using median optical sections in Image J. For all these quantitative analysis, results were presented as mean fluorescence intensity per pixel with standard error of mean. Statistical analysis was done using the Student's *t*-test. For each independent experiment images were taken using the same microscopy settings, and to compare the pixel intensities between wild type and mutants. The same root region was imaged .

### **Förster (Fluorescence) Resonance Energy Transfer (FRET)**

For the initial FRET analysis on the interaction between PID and TCH3, protoplasts were prepared and their fluorescence monitored using a Leica DM IRBE confocal laser scanning microscope with a 63x water objective. The fluorescence was visualized with an Argon laser for excitation at 514 nm (YFP) and 457 nm (CFP) with 522-532 nm (for the YFP) and 471-481 nm (for the CFP) emission filters. FRET studies on the interaction between PID and TCH3 were done by excitation at 457 nm (donor, CFP) and by measuring emission at 475 and 529 nm using a RSP 465 filter. The intensity of three

fixed areas (regions of interest, ROIs) was quantified using the Leica confocal laser scanning software. The fluorescence intensities of these three ROIs was averaged and normalized, and used to calculate the slope of the line from 475 to 529 nm. Per sample three protoplasts were analysed, and the obtained slope values for the three protoplasts was averaged and used to calculate the standard deviation. The Student's *t*-test was used to test for significant differences in slope value between the test sample and the negative control. A significantly reduced slope value (because of a quenched donor emission wavelength intensity, combined with an increased acceptor emission wavelength intensity) was considered indicative for protein-protein interaction-dependent FRET. Similar results were obtained for three independent transfections.

Later FRET studies on the interaction between TCH3 and other AGC3 kinases were done using a sensitized emission FRET approach. Protoplasts were prepared by PEG-mediated transfection. All microscopic analyses were done with confocal laser scanning microscopy (CLSM) using a Zeiss LSM5 Exciter (Zeiss, Oberkochen, Germany) using a 63x magnifying objective. CFP signal was detected using an argon 458 nm laser and 475-525 nm band pass filter. YFP signal was detected using an argon 514 nm laser and a 530-600 nm band pass filter. To detect FRET signal a 458 nm laser and a 530 nm long pass filter were used. To quantify FRET by sensitized emission, the Image J plugin 'FRET and Colocalization Analyzer' was used. This plugin allows calculation of a FRET index on a pixel by pixel basis and corrects for donor bleed through, acceptor bleed through and false FRET (by associating FRET with colocalization of the two fluophores). A "donor only" protoplast expressing *35S::CFP* and an "acceptor only" protoplast expressing *35S::YFP* were used to determine donor bleed through and acceptor bleed through, respectively. The *35S::CFP-YFP* fusion construct was used as a positive control. The plugin was used to calculate the FRET index image, and the relative FRET image was obtained by dividing the FRET index image by the YFP channel image. Three regions of interest (ROIs) were quantified using the ImageJ software. Per sample scanning was performed on ten protoplasts. The obtained intensity of all protoplasts was averaged and used to calculate the standard deviation. The Student's *t*-test was used to test for significant differences in relative FRET ( $p < 0.05$ ).

### **Protein biochemistry**

*In vitro* pull-down analysis was performed as previously described (Benjamins et al., 2003).

For PepChip phosphorylation assays, His-tagged proteins were purified by immobilized-metal affinity chromatography. Bacterial pellets were resuspended in 2 ml of Lysis Buffer (LB: 25 mM Tris pH 8.0, 500 mM NaCl, 20 mM imidazole, 0.05 % Tween-20, 10 % glycerol) and incubated 5 min on ice. After sonication for 2 min, 100  $\mu$ l of 20 % Triton X-100 was added and the mixture was incubated 5 min on ice, followed by centrifugation at 10000 g for 15 min at 4 °C. The soluble fraction was added with 400  $\mu$ l of pre-equilibrated 50 % NTA-agarose matrix (Qiagen) and mixed gently for 1.5 h at 4 °C. Beads were washed three times with 2 ml of LB, 2 ml of Washing Buffer 3 (25 mM Tris pH 7.5, 500 mM NaCl, 40 mM imidazole, 0.01 % Tween-20, 10 % glycerol), and 2 ml of Wash Buffer 4 (25 mM Tris pH 7.0, 500 mM NaCl, 80 mM imidazole and 10 % glycerol). Elution was performed by incubating the beads on 600  $\mu$ l Elution Buffer 2 (25 mM Tris pH 7.0, 300 mM NaCl, 300 mM imidazole, 10 % glycerol) for 30 min at 4 °C. Samples were analyzed by SDS-PAGE and quantified.

The Pepchip Kinase Slide A (Pepscan) was used for *in vitro* phosphorylation assays for PID in the presence of TCH3. Thirty ng of His:PID, His:TCH3 and His:PBP1 were mixed with Kinase Mastermix (50 mM HEPES pH 7.4, 20 mM MgCl<sub>2</sub>, 20 % v/v glycerol, 0.01 mg/ml BSA, 0.01 % v/v Brij-35, 2 mM CaCl<sub>2</sub>), 10  $\mu$ M ATP and 300  $\mu$ Ci/ml  $\gamma$ -33P-ATP (specific activity ~ 3000 Ci/mmol, Amersham). Fifty  $\mu$ l of the reaction mix was incubated with the Pepchip Kinase Slide A for 4 h at 30 °C in a humid chamber. Slides were washed twice with 2 M NaCl, twice with water and dried for 30 min. Slides were exposed to X-ray film FUJI Super RX for 12 and 24 h. The intensity of the signal was quantified by densitometry analysis within uniform circles placed on the peptide spots using ImageQuant software (Molecular Dynamics)

### **RNA extraction and Northern Blots**

Total RNA was purified using the RNeasy Plant Mini kit (Qiagen). Subsequent RNA blot analysis was performed as described (Memelink et al., 1994) using 10  $\mu$ g of total RNA per sample. The following modifications were made: pre-hybridizations and hybridizations were conducted at 65 °C in 2xSSPE 0.5% SDS, and for 20 min at 42 °C in respectively 0.2x SSPE 0.5% SDS, 0.1xSSPE 0.5% SDS and 0.1x SSPE. Blots were exposed to X-ray film FUJI Super RX. The probes for *AtROC5*, for  *$\alpha$ Tubulin* and *PID* were PCR amplified from *Arabidopsis thaliana* Col-0 genomic DNA and column purified (Qiagen). Probes were radioactively labeled using a Prime-a-gene kit (Promega).

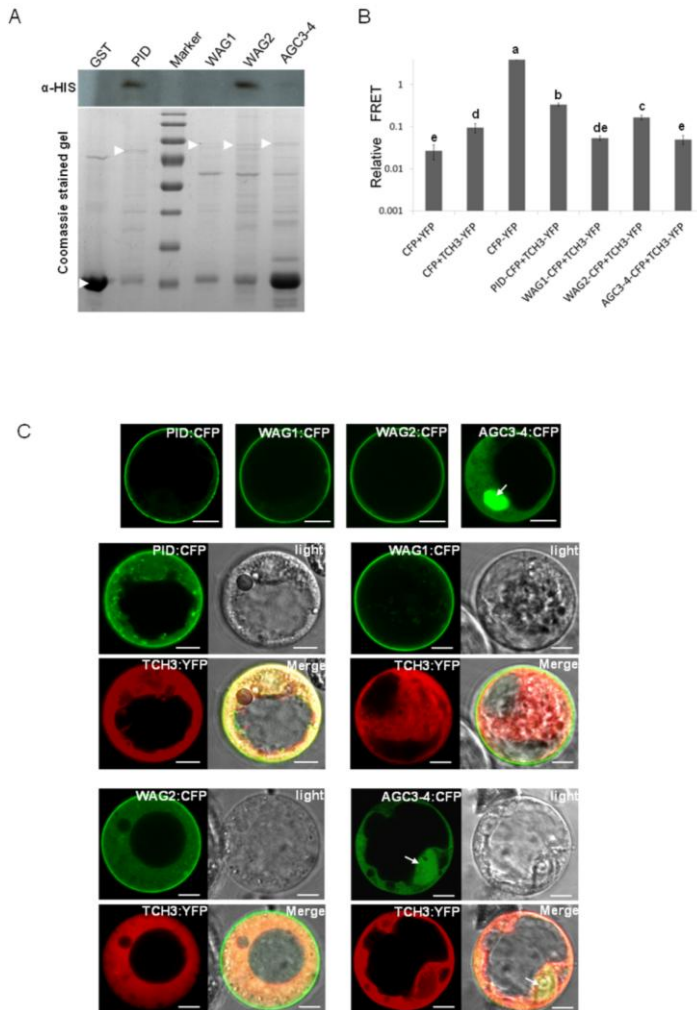
### **Accession numbers**

The *Arabidopsis* Genome Initiative locus identifiers for the genes mentioned are as follows: *PBP1* (At5g54490), *PID* (At2g34650), *WAG1* (At1g5700), *WAG2* (At3g14370), *AGC3-4* (At2g26700), *TCH3* (At2g41100), *ROC* (At4g38740), *PIN2* (At5g57090), *αTubulin* (At5g44340).

### **Acknowledgments**

The authors would like to thank Marcus Heisler for kindly providing the *PID::PID-VENUS* line, Janet Braam for sharing her unpublished data on the *tch3-3* allele, Teva Vernoux for providing the *35S::DII:VENUS* line, Jiri Friml for sharing the *abp1-5* mutant, and Katherine Perrot-Rechenmann for sharing the ethanol inducible SS12S6, SS12K9 lines. Also, we thank Jos Joore for support with the Pepchip Kinase experiments. We are indebted to Gerda Lamers, Ward de Winter and Jan Vink for their help with the microscopy, tissue culture and plant caretaking, respectively.

The project was supported by a grant to R.O. from the Research Council of Chemical Sciences (NWO-CW TOP 700.58.301) with financial support from the Netherlands Organisation for Scientific Research (NWO); C.G.A. was supported by a grant to RO from the Research Council for Earth and Life Sciences (ALW 813.06.004) with financial support from the Netherlands Organisation for Scientific Research (NWO).

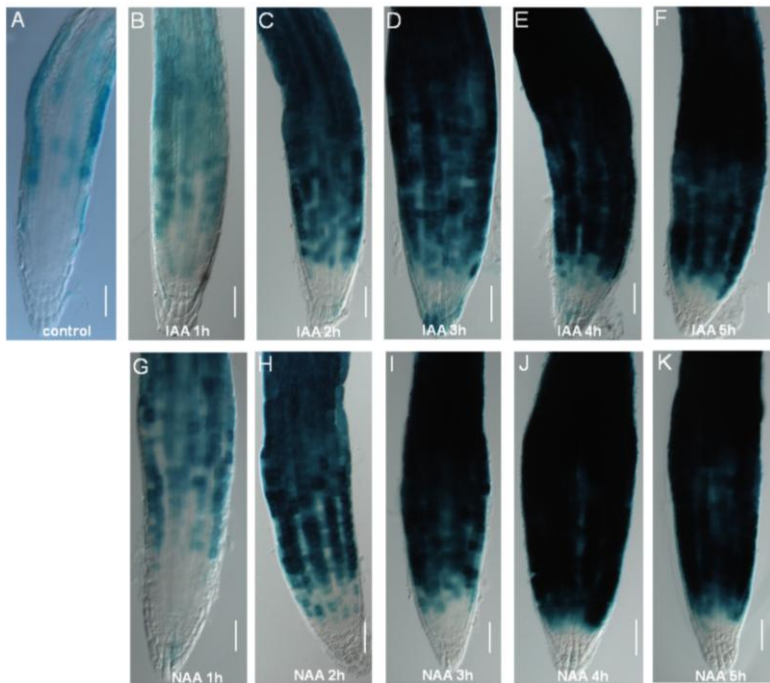


**Supplementary Figure S1 TCH3 interacts with PID and WAG2, but not with the other two AGC3 kinases.**

(A) Western blot analysis of an *in vitro* pull down of His-tagged TCH3 with GST-tagged PID, WAG1, WAG2 or AGC3-4 using anti-His antibodies (upper panel). The lower panel shows the coomassie stained gel used for the Western blot.

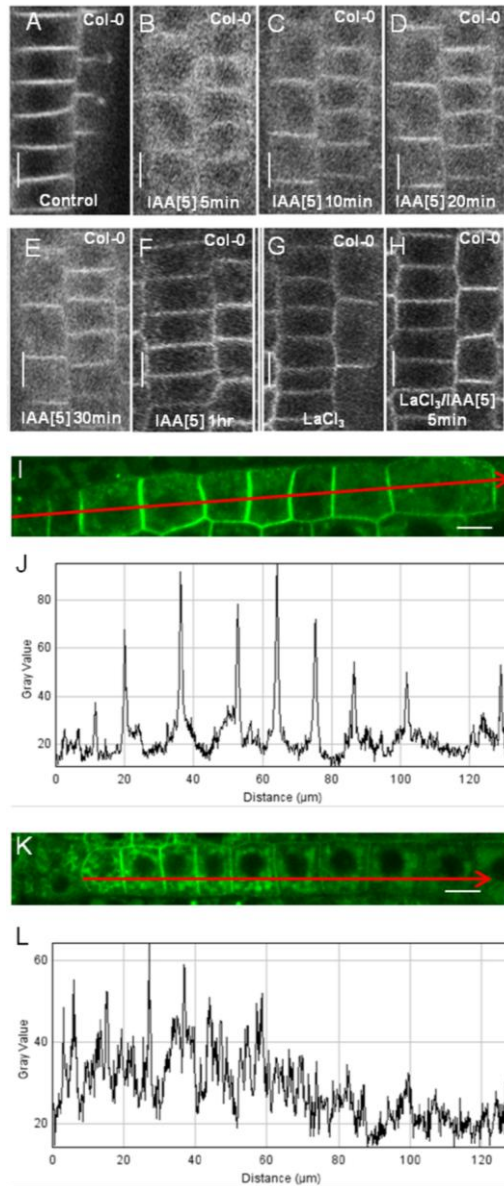
(B, C) Sensitized emission FRET analysis on protoplasts co-expressing TCH3:YFP and PID:CFP, WAG1:CFP, WAG2:CFP or AGC3-4:CFP. The relative FRET index was determined by three measurements in ten co-expressing protoplasts. (B). A log<sup>10</sup> scale is used for the Y axis. Error bars represent the standard error of

the mean. The significantly different classes are indicated with a to e ( $p < 0.05$ ,  $t$ -test). (C) Confocal images of protoplasts showing the CFP channel image for single transfected protoplasts and the CFP-, YFP- and transmitted light channel images and a merged picture of these three images for the double transfected protoplasts. Scale bar indicates 10  $\mu\text{m}$ . CFP and FRET signals were collected simultaneously, and the YFP signal was collected separately.



**Supplementary Figure S2 Auxin-induced *TCH3* expression in the root tip**

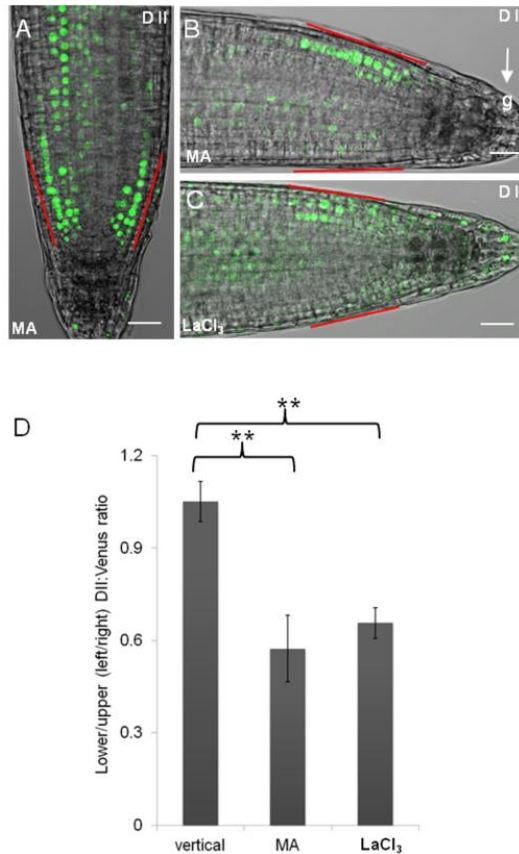
(A-K) Images of histochemically stained *TCH3:TCH3-GUS* seedling root tips that were mock treated (A), or treated for 1 to 5 hours with 5  $\mu\text{M}$  IAA (B-F) or 5  $\mu\text{M}$  NAA (G-K).



**Supplementary Figure S3 The natural auxin indole-3-acetic acid (IAA) induces transient PID dissociation from the plasma membrane (PM).**

(A-H) PID dissociates from the PM after 5 minutes treatment with 5 μM IAA (B), but gradually returns to the PM between 10 to 60 minutes after IAA treatment (C to F). Pretreatment for 30 minutes with LaCl<sub>3</sub> (G) does

not influence PID localization, but blocks the auxin-induced dissociation of PID from the PM (5 minutes with 5  $\mu$ M IAA, H). (I-L) Quantification of the PID-VENUS signal in a root epidermis cell file of untreated (I,J) or 5  $\mu$ M IAA treated (K,L) root tips using Image J software (J,L).



**Supplementary Figure S4  $\text{Ca}^{2+}$  acts downstream of the differential auxin distribution during gravitropic root growth.**

(A-D) Auxin distribution in *Arabidopsis* root tips, as indicated by the auxin response reporter *35S::DII-VENUS*. Roots were grown vertically (A) or gravistimulated for 1 hour on control MA medium (B) or on MA medium supplemented with 1.25 mM  $\text{LaCl}_3$  (C). Quantification of the DII-VENUS signal in the lateral root cap on the upper and lower side of the root tip (D). Red lines in A to C indicate the measured area.

Error bars in D represents the standard error of the mean, \* $p < 0.05$ ; \*\* $p < 0.01$  ( $t$  test). Scale bar in A to C is 20  $\mu\text{m}$ .

## Reference

- Abas, L., Benjamins, R., Malenica, N., Paciorek, T., Wisniewska, J., Moulinier-Anzola, J.C., Sieberer, T., Friml, J., and Luschnig, C.** (2006). Intracellular trafficking and proteolysis of the *Arabidopsis* auxin-efflux facilitator PIN2 are involved in root gravitropism. *Nat Cell Biol* **8**, 249-256.
- Antosiewicz, D.M., Polisensky, D.H., and Braam, J.** (1995). Cellular localization of the Ca<sup>2+</sup> binding TCH3 protein of *Arabidopsis*. *Plant J* **8**, 623-636.
- Antosiewicz, D.M., Purugganan, M.M., Polisensky, D.H., and Braam, J.** (1997). Cellular localization of *Arabidopsis* xyloglucan endotransglycosylase-related proteins during development and after wind stimulation. *Plant Physiol* **115**, 1319-1328.
- Band, L.R., Wells, D.M., Larrieu, A., Sun, J., Middleton, A.M., French, A.P., Brunoud, G., Sato, E.M., Wilson, M.H., Peret, B., Oliva, M., Swarup, R., Sairanen, I., Parry, G., Ljung, K., Beeckman, T., Garibaldi, J.M., Estelle, M., Owen, M.R., Vissenberg, K., Hodgman, T.C., Pridmore, T.P., King, J.R., Vernoux, T., and Bennett, M.J.** (2012). Root gravitropism is regulated by a transient lateral auxin gradient controlled by a tipping-point mechanism. *Proc Natl Acad Sci U S A* **109**, 4668-4673.
- Baster, P., Robert, S., Kleine-Vehn, J., Vanneste, S., Kania, U., Grunewald, W., De Rybel, B., Beeckman, T., and Friml, J.** (2013). SCF<sup>TIR1/AFB</sup>-auxin signalling regulates PIN vacuolar trafficking and auxin fluxes during root gravitropism. *EMBO J* **32**, 260-274.
- Baum, G., Long, J.C., Jenkins, G.I., and Trewavas, A.J.** (1999). Stimulation of the blue light phototropic receptor NPH1 causes a transient increase in cytosolic Ca<sup>2+</sup>. *Proc Natl Acad Sci U S A* **96**, 13554-13559.
- Benjamins, R., Ampudia, C.S., Hooykaas, P.J., and Offringa, R.** (2003). PINOID-mediated signaling involves calcium-binding proteins. *Plant Physiol* **132**, 1623-1630.
- Benjamins, R., Quint, A., Weijers, D., Hooykaas, P., and Offringa, R.** (2001). The PINOID protein kinase regulates organ development in *Arabidopsis* by enhancing polar auxin transport. *Development* **128**, 4057-4067.
- Benkova, E., Michniewicz, M., Sauer, M., Teichmann, T., Seifertova, D., Jurgens, G., and Friml, J.** (2003). Local, efflux-dependent auxin gradients as a common module for plant organ formation. *Cell* **115**, 591-602.
- Bouché N., Yellin, A., Snedden, W.A., and Fromm, H.** (2005). Plant-specific

calmodulin-binding proteins. *Annu Rev Plant Biol* **56**, 435-466.

**Braam, J., and Davis, R.W.** (1990). Rain-, wind-, and touch-induced expression of calmodulin and calmodulin-related genes in *Arabidopsis*. *Cell* **60**, 357-364.

**Braun, N., Wyrzykowska, J., Muller, P., David, K., Couch, D., Perrot-Rechenmann, C., and Fleming, A.J.** (2008). Conditional repression of AUXIN BINDING PROTEIN1 reveals that it coordinates cell division and cell expansion during postembryonic shoot development in *Arabidopsis* and tobacco. *Plant Cell* **20**, 2746-2762.

**Brunoud, G., Wells, D.M., Oliva, M., Larrieu, A., Mirabet, V., Burrow, A.H., Beeckman, T., Kepinski, S., Traas, J., Bennett, M.J., and Vernoux, T.** (2012). A novel sensor to map auxin response and distribution at high spatio-temporal resolution. *Nature* **482**, 103-106.

**Chen, J.G., Ullah, H., Young, J.C., Sussman, M.R., and Jones, A.M.** (2001). ABP1 is required for organized cell elongation and division in *Arabidopsis* embryogenesis. *Genes Dev* **15**, 902-911.

**Cheng, S.H., Willmann, M.R., Chen, H.C., and Sheen, J.** (2002). Calcium signaling through protein kinases. The *Arabidopsis* calcium-dependent protein kinase gene family. *Plant Physiol.* **129**, 469-485.

**Clough, S.J., and Bent, A.F.** (1998). Floral dip: a simplified method for *Agrobacterium*-mediated transformation of *Arabidopsis thaliana*. *Plant J* **16**, 735-743.

**Corbalan-Garcia, S., Guerrero-Valero, M., Marin-Vicente, C., and Gomez-Fernandez, J.C.** (2007). The C2 domains of classical/conventional PKCs are specific PtdIns(4,5)P(2)-sensing domains. *Biochem Soc Trans* **35**, 1046-1048.

**Dahlke, R.I., Luethen, H., and Steffens, B.** (2010). ABP1: an auxin receptor for fast responses at the plasma membrane. *Plant Signal Behav* **5**, 1-3.

**Darwin, C.** (1880). *The power of movement in plants*. London: John Murray.

**David, K.M., Couch, D., Braun, N., Brown, S., Grosclaude, J., and Perrot-Rechenmann, C.** (2007). The auxin-binding protein 1 is essential for the control of cell cycle. *Plant J* **50**, 197-206.

**dela Fuente, R.K., and Leopold, A.C.** (1973). A role for calcium in auxin transport. *Plant Physiol* **51**, 845-847.

**Dhonukshe, P., Huang, F., Galvan-Ampudia, C.S., Mahonen, A.P., Kleine-Vehn, J., Xu, J., Quint, A., Prasad, K., Friml, J., Scheres, B., and Offringa, R.** (2010). Plasma membrane-bound AGC3 kinases phosphorylate PIN auxin carriers at TPRXS(N/S)

motifs to direct apical PIN recycling. *Development* **137**, 3245-3255.

**Ding, Z., Galván-Ampudia, C.S., Demarsy, E., Langowski, L., Kleine-Vehn, J., Fan, Y., Morita, M.T., Tasaka, M., Fankhauser, C., Offringa, R., and Friml, J.** (2011). Light-mediated polarization of the PIN3 auxin transporter for the phototropic response in *Arabidopsis*. *Nat Cell Biol* **13**, 447-452.

**Esmon, C.A., Tinsley, A.G., Ljung, K., Sandberg, G., Hearne, L.B., and Liscum, E.** (2006). A gradient of auxin and auxin-dependent transcription precedes tropic growth responses. *Proc Natl Acad Sci U S A* **103**, 236-241.

**Felle, H.** (1988). Auxin causes oscillations of cytosolic free calcium and pH in *Zea mays* coleoptiles. *Planta* **174**, 495-499.

**Folta, K.M., Lieg, E.J., Durham, T., and Spalding, E.P.** (2003). Primary inhibition of hypocotyl growth and phototropism depend differently on phototropin-mediated increases in cytoplasmic calcium induced by blue light. *Plant Physiol* **133**, 1464-1470.

**Friml, J.** (2003). Auxin transport - shaping the plant. *Curr Opin Plant Biol* **6**, 7-12.

**Friml, J., Wisniewska, J., Benkova, E., Mendgen, K., and Palme, K.** (2002). Lateral relocation of auxin efflux regulator PIN3 mediates tropism in *Arabidopsis*. *Nature* **415**, 806-809.

**Friml, J., Vieten, A., Sauer, M., Weijers, D., Schwarz, H., Hamann, T., Offringa, R., and Jurgens, G.** (2003). Efflux-dependent auxin gradients establish the apical-basal axis of *Arabidopsis*. *Nature* **426**, 147-153.

**Friml, J., Yang, X., Michniewicz, M., Weijers, D., Quint, A., Tietz, O., Benjamins, R., Ouwerkerk, P.B., Ljung, K., Sandberg, G., Hooykaas, P.J., Palme, K., and Offringa, R.** (2004). A PINOID-dependent binary switch in apical-basal PIN polar targeting directs auxin efflux. *Science* **306**, 862-865.

**Galván-Ampudia, C.S., and Offringa, R.** (2007). Plant evolution: AGC kinases tell the auxin tale. *Trends Plant Sci.* **12**, 541-547.

**Gehring, C.A., Irving, H.R., and Parish, R.W.** (1990a). Effects of auxin and abscisic acid on cytosolic calcium and pH in plant cells. *Proc Natl Acad Sci U S A* **87**, 9645-9649.

**Gehring, C.A., Williams, D.A., Cody, S.H., and Parish, R.W.** (1990b). Phototropism and geotropism in maize coleoptiles are spatially correlated with increases in cytosolic free calcium. *Nature* **345**, 528-530.

**Guan, K.L., and Dixon, J.E.** (1991). Eukaryotic proteins expressed in *Escherichia coli*: an improved thrombin cleavage and purification procedure of fusion proteins with

glutathione S-transferase. *Anal Biochem* **192**, 262-267.

**Harada, A., and Shimazaki, K.** (2007). Phototropins and blue light-dependent calcium signaling in higher plants. *Photochem Photobiol* **83**, 102-111.

**Harada, A., Sakai, T., and Okada, K.** (2003). phot1 and phot2 mediate blue light-induced transient increases in cytosolic Ca<sup>2+</sup> differently in *Arabidopsis* leaves. *Proc Natl Acad Sci U S A* **100**, 8583-8588.

**Hashimoto, K., and Kudla, J.** (2011). Calcium decoding mechanisms in plants. *Biochimie* **93**, 2054-2059.

**Hellens, R.P., Edwards, E.A., Leyland, N.R., Bean, S., and Mullineaux, P.M.** (2000). pGreen: a versatile and flexible binary Ti vector for *Agrobacterium*-mediated plant transformation. *Plant Mol Biol* **42**, 819-832.

**Hood, E., Gelvin, S., Melchers, L., and Hoekema, A.** (1993). New *Agrobacterium* helper plasmids for gene transfer to plants. *Transgenic Research* **2**, 208-218.

**Huang, F., Zago, M.K., Abas, L., van Marion, A., Galvan-Ampudia, C.S., and Offringa, R.** (2010). Phosphorylation of conserved PIN motifs directs *Arabidopsis* PIN1 polarity and auxin transport. *Plant Cell* **22**, 1129-1142.

**Kleine-Vehn, J., Ding, Z., Jones, A.R., Tasaka, M., Morita, M.T., and Friml, J.** (2010). Gravity-induced PIN transcytosis for polarization of auxin fluxes in gravity-sensing root cells. *Proc Natl Acad Sci U S A* **107**, 22344-22349.

**Korasick, D.A., Enders, T.A., and Strader, L.C.** (2013). Auxin biosynthesis and storage forms. *J Exp Bot* **64**, 2541-2555.

**Lariguet, P., Schepens, I., Hodgson, D., Pedmale, U.V., Trevisan, M., Kami, C., de Carbonnel, M., Alonso, J.M., Ecker, J.R., Liscum, E., and Fankhauser, C.** (2006). PHYTOCHROME KINASE SUBSTRATE 1 is a phototropin 1 binding protein required for phototropism. *Proc Natl Acad Sci U S A* **103**, 10134-10139.

**Lee, J.S., and Evans, M.L.** (1985). Polar transport of auxin across gravistimulated roots of maize and its enhancement by calcium. *Plant Physiol* **77**, 824-827.

**Lee, J.S., Mulkey, T.J., and Evans, M.L.** (1984). Inhibition of polar calcium movement and gravitropism in roots treated with auxin-transport inhibitors. *Planta* **160**, 536-543.

**Lee, S.H., and Cho, H.T.** (2006). PINOID positively regulates auxin efflux in *Arabidopsis* root hair cells and tobacco cells. *Plant Cell* **18**, 1604-1616.

**Ljung, K.** (2013). Auxin metabolism and homeostasis during plant development. *Development* **140**, 943-950.

- Luan, S., Kudla, J., Rodriguez-Concepcion, M., Yalovsky, S., and Gruissem, W.** (2002). Calmodulins and calcineurin B-like proteins: calcium sensors for specific signal response coupling in plants. *Plant Cell* **14**, S389-400.
- Masson, J., and Paszkowski, J.** (1992). The culture response of *Arabidopsis thaliana* protoplasts is determined by the growth conditions of donor plants. *The Plant Journal* **2**, 829-833.
- McCormack, E., and Braam, J.** (2003). Calmodulins and related potential calcium sensors of *Arabidopsis*. *New Phytol.* **159**, 585-598.
- McLaughlin, S., and Murray, D.** (2005). Plasma membrane phosphoinositide organization by protein electrostatics. *Nature* **438**, 605-611.
- Memelink, J., Swords, K.M., Staehelin, L.A., and Hoge, J.H.** (1994). Southern, Northern and Western blot analysis. In *Plant Molecular Biology Manual*, S. Gelvin and R. Schilperoort, eds (Springer Netherlands), pp. 273-295.
- Michniewicz, M., Zago, M.K., Abas, L., Weijers, D., Schweighofer, A., Meskiene, I., Heisler, M.G., Ohno, C., Zhang, J., Huang, F., Schwab, R., Weigel, D., Meyerowitz, E.M., Luschnig, C., Offringa, R., and Friml, J.** (2007). Antagonistic regulation of PIN phosphorylation by PP2A and PINOID directs auxin flux. *Cell* **130**, 1044-1056.
- Monshausen, G.B., Messerli, M.A., and Gilroy, S.** (2008). Imaging of the Yellow Cameleon 3.6 indicator reveals that elevations in cytosolic Ca<sup>2+</sup> follow oscillating increases in growth in root hairs of *Arabidopsis*. *Plant Physiol* **147**, 1690-1698.
- Monshausen, G.B., Bibikova, T.N., Weisenseel, M.H., and Gilroy, S.** (2009). Ca<sup>2+</sup> regulates reactive oxygen species production and pH during mechanosensing in *Arabidopsis* roots. *Plant Cell* **21**, 2341-2356.
- Monshausen, G.B., Miller, N.D., Murphy, A.S., and Gilroy, S.** (2011). Dynamics of auxin-dependent Ca<sup>2+</sup> and pH signaling in root growth revealed by integrating high-resolution imaging with automated computer vision-based analysis. *Plant J.* **65**, 309-318.
- Moore, R.** (1985). Calcium movement, graviresponsiveness and the structure of columella cells and columella tissues in roots of *Allium cepa* L. *Annals of Botany* **56**, 173-187.
- Nakajima, K., and Benfey, P.N.** (2002). Signaling in and out: control of cell division and differentiation in the shoot and root. *Plant Cell* **14 Suppl**, S265-276.
- Ottenschlager, I., Wolff, P., Wolvertson, C., Bhalerao, R.P., Sandberg, G., Ishikawa, H., Evans, M., and Palme, K.** (2003). Gravity-regulated differential auxin transport

from columella to lateral root cap cells. *Proc Natl Acad Sci U S A* **100**, 2987-2991.

**Paciorek, T., Zazimalova, E., Ruthardt, N., Petrasek, J., Stierhof, Y.D., Kleine-Vehn, J., Morris, D.A., Emans, N., Jurgens, G., Geldner, N., and Friml, J.** (2005). Auxin inhibits endocytosis and promotes its own efflux from cells. *Nature* **435**, 1251-1256.

**Peret, B., De Rybel, B., Casimiro, I., Benkova, E., Swarup, R., Laplaze, L., Beeckman, T., and Bennett, M.J.** (2009). *Arabidopsis* lateral root development: an emerging story. *Trends Plant Sci.* **14**, 399-408.

**Petrasek, J., and Friml, J.** (2009). Auxin transport routes in plant development. *Development* **136**, 2675-2688.

**Petrasek, J., Mravec, J., Bouchard, R., Blakeslee, J.J., Abas, M., Seifertova, D., Wisniewska, J., Tadele, Z., Kubes, M., Covanova, M., Dhonukshe, P., Skupa, P., Benkova, E., Perry, L., Krecek, P., Lee, O.R., Fink, G.R., Geisler, M., Murphy, A.S., Luschnig, C., Zazimalova, E., and Friml, J.** (2006). PIN proteins perform a rate-limiting function in cellular auxin efflux. *Science* **312**, 914-918.

**Poovalah, B.W., McFadden, J.J., and Reddy, A.S.** (1987). The role of calcium ions in gravity signal perception and transduction. *Physiol Plant* **71**, 401-407.

**Rademacher, E.H., and Offringa, R.** (2012). Evolutionary adaptations of plant AGC Kinases: from light signaling to cell polarity regulation. *Front Plant Sci* **3**, 250.

**Reinhardt, D., Mandel, T., and Kuhlemeier, C.** (2000). Auxin regulates the initiation and radial position of plant lateral organs. *Plant Cell* **12**, 507-518.

**Reinhardt, D., Pesce, E.R., Stieger, P., Mandel, T., Baltensperger, K., Bennett, M., Traas, J., Friml, J., and Kuhlemeier, C.** (2003). Regulation of phyllotaxis by polar auxin transport. *Nature* **426**, 255-260.

**Robert, S., Kleine-Vehn, J., Barbez, E., Sauer, M., Paciorek, T., Baster, P., Vanneste, S., Zhang, J., Simon, S., Covanova, M., Hayashi, K., Dhonukshe, P., Yang, Z., Bednarek, S.Y., Jones, A.M., Luschnig, C., Aniento, F., Zazimalova, E., and Friml, J.** (2010). ABP1 mediates auxin inhibition of clathrin-dependent endocytosis in *Arabidopsis*. *Cell* **143**, 111-121.

**Roux, S.J., and Serlin, B.S.** (1987). Cellular mechanisms controlling light-stimulated gravitropism: role of calcium. *CRC Crit Rev Plant Sci* **5**, 205-236.

**Sabatini, S., Beis, D., Wolkenfelt, H., Murfett, J., Guilfoyle, T., Malamy, J., Benfey, P., Leyser, O., Bechtold, N., Weisbeek, P., and Scheres, B.** (1999). An auxin-dependent distal organizer of pattern and polarity in the *Arabidopsis* root. *Cell* **99**,

463-472.

**Sambrook, J., Fritsch F. and Maniatis, T.** (1989). Molecular cloning-A laboratory manual. Cold Spring Harbor Laboratory press, NY, USA.

**Sanders, D., Pelloux, J., Brownlee, C., and Harper, J.F.** (2002). Calcium at the crossroads of signaling. *Plant Cell* **14 Suppl**, S401-417.

**Sauer, M., Balla, J., Luschnig, C., Wisniewska, J., Reinohl, V., Friml, J., and Benkova, E.** (2006). Canalization of auxin flow by Aux/IAA-ARF-dependent feedback regulation of PIN polarity. *Genes Dev* **20**, 2902-2911.

**Schirawski, J., Planchais, S., and Haenni, A.L.** (2000). An improved protocol for the preparation of protoplasts from an established *Arabidopsis thaliana* cell suspension culture and infection with RNA of turnip yellow mosaic tymovirus: a simple and reliable method. *J Virol Methods* **86**, 85-94.

**Shishova, M., and Lindberg, S.** (2004). Auxin induces an increase of Ca<sup>2+</sup> concentration in the cytosol of wheat leaf protoplasts. *J Plant Physiol* **161**, 937-945.

**Shishova, M., Yemelyanov, V., Rudashevskaya, E., and Lindberg, S.** (2007). A shift in sensitivity to auxin within development of maize seedlings. *J Plant Physiol* **164**, 1323-1330.

**Siegel, R.M., Chan, F.K., Zacharias, D.A., Swofford, R., Holmes, K.L., Tsien, R.Y., and Lenardo, M.J.** (2000). Measurement of molecular interactions in living cells by fluorescence resonance energy transfer between variants of the green fluorescent protein. *Sci STKE* **2000**, p11.

**Sistrunk, M.L., Antosiewicz, D.M., Purugganan, M.M., and Braam, J.** (1994). *Arabidopsis TCH3* encodes a novel Ca<sup>2+</sup> binding protein and shows environmentally induced and tissue-specific regulation. *Plant Cell* **6**, 1553-1565.

**Snedden, W.A., and Fromm, H.** (2001). Calmodulin as a versatile calcium signal transducer in plants. *New Phytol* **151**, 35-66.

**Steffens, B., Feckler, C., Palme, K., Christian, M., Bottger, M., and Luthen, H.** (2001). The auxin signal for protoplast swelling is perceived by extracellular ABP1. *Plant J* **27**, 591-599.

**Strynadka, N.C., and James, M.N.** (1989). Crystal structures of the helix-loop-helix calcium-binding proteins. *Annu Rev Biochem* **58**, 951-998.

**Swanson, S.J., Choi, W.G., Chanoca, A., and Gilroy, S.** (2011). In vivo imaging of Ca<sup>2+</sup>, pH, and reactive oxygen species using fluorescent probes in plants. *Annu Rev Plant Biol* **62**, 273-297.

- Tanaka, H., Dhonukshe, P., Brewer, P.B., and Friml, J.** (2006). Spatiotemporal asymmetric auxin distribution: a means to coordinate plant development. *Cell Mol Life Sci* **63**, 2738-2754.
- Travé G., Lacombe, P.J., Pfuhl, M., Saraste, M., and Pastore, A.** (1995). Molecular mechanism of the calcium-induced conformational change in the spectrin EF-hands. *EMBO J* **14**, 4922-4931.
- Vanneste, S., and Friml, J.** (2009). Auxin: a trigger for change in plant development. *Cell* **136**, 1005-1016.
- Weijers, D., and Jurgens, G.** (2005). Auxin and embryo axis formation: the ends in sight? *Curr Opin Plant Biol* **8**, 32-37.
- Wisniewska, J., Xu, J., Seifertova, D., Brewer, P.B., Ruzicka, K., Blilou, I., Rouquie, D., Benkova, E., Scheres, B., and Friml, J.** (2006). Polar PIN localization directs auxin flow in plants. *Science* **312**, 883.
- Woo, E.J., Marshall, J., Bauly, J., Chen, J.G., Venis, M., Napier, R.M., and Pickersgill, R.W.** (2002). Crystal structure of auxin-binding protein 1 in complex with auxin. *EMBO J* **21**, 2877-2885.
- Xu, J., and Scheres, B.** (2005). Dissection of Arabidopsis ADP-RIBOSYLATION FACTOR 1 function in epidermal cell polarity. *Plant Cell* **17**, 525-536.
- Xu, T., Wen, M., Nagawa, S., Fu, Y., Chen, J.G., Wu, M.J., Perrot-Rechenmann, C., Friml, J., Jones, A.M., and Yang, Z.** (2010). Cell surface- and rho GTPase-based auxin signaling controls cellular interdigitation in *Arabidopsis*. *Cell* **143**, 99-110.
- Xu, T., Dai, N., Chen, J., Nagawa, S., Cao, M., Li, H., Zhou, Z., Chen, X., De Rycke, R., Rakusova, H., Wang, W., Jones, A.M., Friml, J., Patterson, S.E., Bleecker, A.B., and Yang, Z.** (2014). Cell surface ABP1-TMK auxin-sensing complex activates ROP GTPase signaling. *Science* **343**, 1025-1028.
- Zegzouti, H., Anthony, R.G., Jahchan, N., Bogre, L., and Christensen, S.K.** (2006). Phosphorylation and activation of PINOID by the phospholipid signaling kinase 3-phosphoinositide-dependent protein kinase 1 (PDK1) in *Arabidopsis*. *Proc Natl Acad Sci U S A* **103**, 6404-6409.
- Zhao, X., Wang, Y.L., Qiao, X.R., Wang, J., Wang, L.D., Xu, C.S., and Zhang, X.** (2013). Phototropins function in high-intensity blue light-induced hypocotyl phototropism in *Arabidopsis* by altering cytosolic calcium. *Plant Physiol* **162**, 1539-1551.